

Robot navigation using stereo vision and polarization imaging

Arunkumar Pandian

Institut Universitaire de Technologie IUT Le Creusot
Université de Bourgogne

A Thesis Submitted for the Degree of
MSc Erasmus Mundus in Vision and Robotics (VIBOT)

· 2008 ·

Abstract

Autonomous off-road navigation is a highly complicated task for a robot owing to the different kinds of obstacles it could encounter. In-particular, water hazards such as puddles and ponds are very common in outdoor environments and are hard to detect even with ranging devices due to the specular nature of reflection at the air water interface. Though a wide range of techniques such as colour image segmentation, multi-feature based scheme, short wave infrared (SWIR) imagery, thermal infrared imagery have been attempted, a system capable of detecting any water hazard camouflaged by various terrain covers is yet to be developed. This project employing polarization imaging and stereo vision to detect water hazards for robot navigation has been motivated by the fact that the light reflected from static water surfaces is often partially linearly polarized with significant degree of polarization. Starting from the conventional single camera polarization imaging setup employing a mechanically rotated polarizer, several other arrangements such as the polarization contrast imaging using two cameras, a three camera arrangement enabling the complete characterisation of partially linearly polarized light and finally, a four camera arrangement employing two polarizers with identical orientations to help in stereo matching are investigated in this work. The calibration of the camera setups is carried out using the Matlab camera calibration toolbox from Bouguet. The important challenge in the proposed system is to improve the pixel correspondence across the polarization images. Though different matching scores such as the hamming distance from census transformed images and zero mean normalised cross correlation and image post processing technique such as the histogram equalization have been experimented, it is desirable to further improve the stereo matching results in the future works. The four camera arrangement employed in this work was found to fail in the case of water reflecting the surrounding structures but it is required to investigate it in greater detail in the future works. The importance of the four camera arrangement is that it could greatly reduce the complexity involved in matching across the polarization images. The important contributions of this work include the demonstration of the sensory augmentation capabilities of polarization imaging and investigation of its applicability in water detection tasks, the development of Matlab programs to allow graphical selection of pixels and the computation of their matches in other views using various matching scores, the development of a Matlab program to visualise the polarization information using a Hue-Saturation-Intensity representation and finally, the establishment of guidelines for future research in this field.

Contents

Acknowledgments	vii
1 Introduction	1
1.1 Motivations for the project	1
1.2 Contributions of this project	2
1.3 Organisation of the thesis	3
2 Outdoor water hazard detection	4
2.1 Introduction	4
2.2 State-of-the-art outdoor water detection techniques	6
2.2.1 Colour imagery based scheme	6
2.2.2 Multi-feature based water detection techniques	7
2.2.3 Short-Wave Infrared (SWIR) imagery	9
2.2.4 Thermal Infrared Imagery	9
2.2.5 LASER range finder based approach	9
2.3 Summary	10
3 Polarization based vision system for outdoor water hazard detection	11
3.1 Polarization of Light:Background	12
3.1.1 Types of polarized light	12
3.2 Polarization of outdoor light and its analysis	14

3.2.1	Polarization by reflection	15
3.2.2	Analysis of the reflected light using a linear polarizer	17
3.3	Mathematical description of partial linear polarization	19
3.4	Simplified polarization imaging	19
3.4.1	Polarization parameters	19
3.4.2	Polarization imaging cameras	20
3.4.3	Scheme for visualising partial linear polarization	21
3.5	Suitability of a polarization based water cue for outdoor navigation	22
3.6	Survey of polarization imaging based water detection techniques	24
3.7	Challenges involved in a polarization based stereo system	26
3.8	Functional decomposition of the proposed scheme	26
3.9	Summary	27
4	Implementation and performance evaluation of the proposed schemes	28
4.1	Single camera with a rotating polarizer	28
4.2	Stereo cameras with mutually perpendicular fixed polarizers	31
4.2.1	Choice of orientations for the linear polarizers	32
4.2.2	Stereo camera calibration	32
4.2.3	Stereo matching using epipolar geometry	33
4.2.4	Choice of the matching score	33
4.2.5	Analysis of the stereo matching results	36
4.2.6	Polarization contrast image	36
4.2.7	Limitations of a stereo polarization imager	38
4.3	Water detection using multi-camera polarization imaging	39
4.3.1	Four camera polarization imaging arrangement	39
4.3.2	The minimum resource required for optimal performance in water detection tasks	41
4.3.3	Water detection using three polarization images	41

4.4 Summary	44
5 Conclusion and scope for future work	47
A Derivation of the Brewster's angle from Snell's law	49
B Derivation of the polarization parameters	50
C Description of the camera calibration procedure	51
Bibliography	55

List of Figures

2.1	An outdoor scene with a large body of water reflecting different parts of the scene namely, the sky and the surrounding vegetation	5
2.2	An Image from the DARPA 2004 Grand Challenge media gallery showing a course terrain with water	6
3.1	Linear, Circular and Elliptical polarization [8]	12
3.2	Electric field vector distribution in a circularly polarized light [8]	14
3.3	Distribution of electric field vectors in an unpolarized and partially linearly polarized light [8]	14
3.4	Reflection and Refraction at an interface between two media with different refractive indices	16
3.5	Reflected intensity for rays parallel and perpendicular to the plane of incidence. . . .	17
3.6	Variation of the degree of polarization with angle of incidence of the light reflected at an air-water interface	18
3.7	Reflected intensity for rays parallel and perpendicular to the plane of incidence. . . .	18
3.8	Images corresponding to intensity, degree and angle of polarization respectively. . . .	22
3.9	HSV colour scale based representation of polarization parameters.	22
3.10	Variation of the angle of polarization of the reflected light with that of the incident light having a partial polarization of 0.8 and with angles of incidence equal to 40, 50, 60 and 70 degrees.	24

3.11	Variation of the angle of polarization of the reflected light with the degree of polarization of the incident light having an angle of polarization of 80 degrees and different angles of incidence, namely 20, 40 and 60 degrees.	24
3.12	Stereo images of an outdoor scene taken from two cameras mounted with polarizers oriented along horizontal and vertical directions highlighting the marked change in intensity of the pixels across the views.	26
3.13	Processing blocks of the proposed water hazard detection system.	27
4.1	Images of a scene recorded with polarizers oriented along 0, 45 and 90 degrees with respect to the horizontal respectively.	29
4.2	Partial polarization, Angle of polarization and Intensity images.	30
4.3	HSV representation of the polarization image.	30
4.4	Original colour image corresponding to a horizontally (0°) oriented polarizer.	31
4.5	Possible results for stereo matching.	35
4.6	The stereo images acquired with approximately perpendicular polarizers, the values of ZNCC along the epipolar line and along the set of rows adjacent to the calculated epipolar line and the unicity constraint validation using the ZNCC scores along the epipolar line of the matched pixel.	37
4.7	The stereo images acquired with approximately perpendicular polarizers, the values of hamming distance along the epipolar line and along the set of rows adjacent to the calculated epipolar line and the unicity constraint validation using the hamming distance scores along the epipolar line of the matched pixel.	38
4.8	Two different schemes for visualizing the polarization contrast computed within a square neighbourhood around the valid stereo matches.	39
4.9	The four IEEE 1394 cameras interfaced through the ports in the mobile robot Dala (LAAS, CNRS) and the view of the cameras from behind showing the calibration of the polarizers.	40
4.10	Images of the calibration grid corresponding to the four cameras.	40

4.11	A shallow body of water reflecting the surrounding mesh and other nearby structures. .	41
4.12	Images captured with polarizers oriented along 90° , 90° , 45° and 0° , with respect to the horizontal respectively.	42
4.13	Water region clipped from the images obtained with different polarizers oriented at 90° , 90° , 45° and 0° with respect to the horizontal and their respective histograms. . . .	43
4.14	The water regions after applying histogram equalization.	43
4.15	Top and bottom rows correspond to the water regions before and after applying histogram equalization to the entire images respectively.	44
4.16	The epipolar lines corresponding to the chosen pixels in the top left image are displayed in the other three images.	45
4.17	The pixels correspondences across the four images with the inliers marked manually using rectangles.	46
4.18	HSV representation of the polarization parameters for every pixel within 11x11 square windows around the selected pixels.	46
C.1	Image of the calibration grid captured from the left and right cameras of a stereo rig. .	52

Acknowledgments

I feel extremely lucky to have had the opportunity of working under the joint supervision of Dr. Olivier MOREL (Le2i) and Dr. Simon LACROIX (LAAS, Toulouse). I am highly grateful to both of them for having offered access to the facilities at Le2i and LAAS, for being flexible with my schedule and above all, for their valuable guidance and constructive critiques. Their willingness to clarify my doubts and even explain basic concepts that I was ignorant of amidst busy schedule and their amiable disposition deserve a special mention.

I am highly indebted to Heriot-Watt University, Universitat de Girona and Univesité de Bourgogne for having helped me realise my dream of pursuing high studies abroad and to the European Commission for having sponsored my education. I take this opportunity to thank all the staff of my master's course for having empowered me with the background knowledge required to carry out my thesis and in-particular the course coordinator, Dr. Fabrice MERI-AUDEAU, for caring so much about the students of my masters programme. I would like to say "Merci beaucoup" to Ms. Valérie Torres for all her help with the administrative tasks.

I would like to thank my fellow Vibot-ians for their excellent company during the past two years. My father's principles, mother's motivation, sister's caring words, grandfather's wishes, grandmother's prayers and uncle's guidance have played a crucial role in shaping my career and I express my heartfelt gratitude to them. I am highly indebted to my homeland, India, for having imparted me quality education and laid the foundation for my career. And finally, I thank the scientific and engineering communities for having put in great effort to bring the indispensable modern technologies including the internet and the computers into existence.

Chapter 1

Introduction

Over the past few years, there has been a growing interest in empowering robots with autonomous off-road navigation capability. The response to the Civilian-European Land Robot Trial (C-ELROB), Military-European Land Robot Trial (M-ELROB) and the Defense Advanced Research Projects Agency (DARPA) grand challenge confirm the above statement. In the 2001 Defense Authorization Act, the U.S. Congress has set a goal that by 2015 one third of their operational ground vehicle will be unmanned. The interest in applying autonomous robots to a wide range of tasks ranging from civil applications such as wide-area environment monitoring, disaster recovery and search-and-rescue activities, to planetary explorations in-addition to military operations, has fuelled the research in this domain. As a result, modern robots are attempting to tackle the challenging task of traversing off-road environments where the terrain is irregular and potential hazards are aplenty.

1.1 Motivations for the project

The ability of a robot or an Unmanned Ground Vehicle (UGV) to accurately sense its environment and use that information for control is of supreme importance in autonomous navigation. In the absence of such sensing capability, the robot has to solely rely on prior knowledge of the environment and on self-localization techniques such as the Global Positioning System (GPS). However, the resolutions offered by GPS and environment maps are considered to be too low for use in obstacle avoidance, which is of prime importance in autonomous navigation. Also, in the case of changing environmental conditions, reference maps are rendered futile. Thus, an efficient sensing of the environment is essential for success in autonomous navigation tasks. The complication involved in environmental sensing is the absence of any correspondence between the geometry and the nature of different obstacles. For example, a water surface or a road or a

meadow or a river bed may have a similar geometry of being approximately flat when observed from a distance but certainly differ in their nature of being traversable or not. Therefore, developing an ability to sense the physical nature of an obstacle by observing it from a certain distance will save the autonomous vehicle from potential hazards. Augmenting the environment sensing capability of an autonomous robot forms the kernel of this thesis work.

An off-road environment is more challenging to traverse compared to an indoor or urban setting owing to its irregular terrain. Also, it is abound with a variety of hazards including water, vegetation, negative obstacles (ditches), mud, snow and fog. Of all these hazards, water hazards such as ponds and puddles have to be considered with high importance due to their common occurrence and elusiveness to common detection techniques. Detecting water in a scene by image segmentation is complicated by the fact that unlike common obstacles which are higher than the ground, water hazards do not have any obvious geometric feature or unique colour (water surfaces take on the colour of the scene elements they are reflecting.). Also, a ranging device such as a LASER or LADAR usually returns a void for the region of the image with the water body due to the signal not getting reflected back to the sensor.

1.2 Contributions of this project

The strategy employed in this work is to exploit the information offered by the polarization state of the light reflected by a water surface. As commercial CCD or CMOS Cameras are capable of recording only the intensity of the incident light, the polarization information is essentially a sensory augmentation with the potential to be applied in outdoor water detection.

The main contributions of this project include the:

- The demonstration of sensory augmentation capabilities of polarization imaging and a detailed investigation of its applicability in water detection tasks
- Analysis of different stereo matching techniques to determine the optimal approach for use in polarization imaging
- A detailed review of the state-of-the-art outdoor water detection techniques
- *Two camera setup*: Development of a Matlab program which permits the graphical selection of interest points on a stereo rectified image and hence displays the stereo correspondences on the other images computing using ZNCC (Zero mean Normalized Cross Correlation) or Hamming distance (Census transform) scores and the calibration results
- *Four camera setup*: Development of a Matlab program which permits the graphical selection of interest points on one of the “four” images obtained using a four camera setup and

hence displays the epipolar lines on the other images computed based on the calibration results. The correspondences could be computed either using ZNCC or using Hamming distance and resulting matches are displayed.

- Development of a Matlab program to display the polarization information using the HSV representation proposed by L.B.Wolff
- Development of a GUI using Matlab Guide tool to study the polarization state of the reflected light
- The calibration of the camera setups using the toolbox from Y.Bouguet.
- The manual labelling of the transmission axes of the rotating polarizers and also the angles with respect to their transmission axes.

1.3 Organisation of the thesis

Chapter 1 [Introduction] has highlighted the growing interest in the field of autonomous off-road navigation in recent times. It has also offered a generic insight into the factors that have motivated this thesis work, namely, the need for augmenting the environment sensing capability of a robot and the high degree of elusiveness exhibited by the hazards present in an off-road environment.

Chapter 2 [General problem formulation] addresses the problem of water detection in outdoor environments and its associated difficulties. A review of the techniques developed to solve the problem of water detection in outdoor environments is provided in this chapter.

Chapter 3 [Polarization background and an overview of the proposed scheme] explains the background theory related to the polarization of light, the phenomenon of polarization by reflection and polarization imaging. Following an analysis of the suitability of applying a polarization based water cue, a review of the water detection techniques based on polarization imaging is provided. It concludes with an overview of the proposed scheme.

Chapter 4 [Implementation and performance analysis of the proposed scheme] discusses the different polarization imaging arrangements that are implemented to determine the setup suited for water hazard detection in outdoor environments. A critical analysis of the performance of these arrangements is discussed and the minimum resources required for acceptable performance are derived at the end of this chapter.

Chapter 5 [Conclusion and scope for future work] This chapter presents the concluding remarks and also an insight into the likely paths for future research in this field.

Chapter 2

Outdoor water hazard detection

Water hazards such as puddles and ponds are one of the most challenging obstacles commonly encountered in outdoor environments. A literature review reveals that only a limited number of works on detecting water hazards or on estimating the depth of potential water hazards exist today. Hence, it could be inferred that there is still plenty of scope for research in the field of outdoor water hazard detection. A detailed description of the complications involved in water hazard detection along with the state-of-the-art techniques addressing this issue are provided in this chapter. As this thesis work concerns the application of information from polarization in water detection, the state-of-the-art water detection techniques based on polarization are discussed following the information on the basic principles of polarization in the next chapter (Chapter 3).

2.1 Introduction

As traversing through deep water bodies could damage an UGV, it is preferable to locate them from a distance that is large enough to steer the vehicle away from them. But, unfortunately, the detection of water hazards in an outdoor environment is complicated due to the reasons detailed below.

The simplest case is the detection of water without any vegetation during the day under a clear sky when most of the water surface reflects the sky and hence, could be identified using colour and brightness information. However, the appearance of water bodies can vary greatly, depending on the following factors:

- scene elements reflected by the surface (sky, vegetation or buildings)
- depth

- size (a pond versus a lake)
- turbidity
- ambient light (day versus night operation)
- presence or absence of ripples on the surface
- surface vegetation and
- shadows

As a result, it is highly challenging to formulate a single feature capable of characterizing water under the different scenarios listed above. Two examples illustrating the challenges involved in detecting water bodies are shown in 2.1 and 2.2. Algorithms based on colour image segmentation are not capable of distinguishing between the vegetation and its reflection on water seen in 2.1. Detection of water body shown in 2.2 is even more complicated than 2.1 as there are changes in illumination along the body of water and are not clearly distinguished from the surrounding terrain.



Figure 2.1: An outdoor scene with a large body of water reflecting different parts of the scene namely, the sky and the surrounding vegetation



Figure 2.2: An Image from the DARPA 2004 Grand Challenge media gallery showing a course terrain with water

2.2 State-of-the-art outdoor water detection techniques

Environment sensing techniques can be broadly classified into passive and active techniques based on whether they employ a source of radiation or not. For example, a stereo vision system employing colour image processing or a system based on short-wave infrared camera are examples of passive sensing techniques. On the other hand, LASER range finders shine a LASER beam and analyse the reflected beam to sense the environment and hence, could be termed as an active technique. A detailed survey of the state-of-the-art techniques concerned with the application of active or passive sensing technologies in outdoor water hazard detection is provided in the subsequent sections.

2.2.1 Colour imagery based scheme

Passive sensing techniques are particularly preferable in military applications as they obviate the emission of detectable electromagnetic signals. Colour cameras are passive sensing devices with the added advantages of being cheap, small and light. As colour image segmentation is considered to be versatile in characterising various obstacles including grass, foliage, soil, dry vegetation and rocks, its application in water hazard detection has been studied in [21].

According to [21], in many off-road conditions, water bodies reflecting the sky could be easily distinguished from other terrain by their colour and brightness, regardless of whether the sky is clear, partly cloudy, or completely overcast and regardless of the surface wave state of water. The brightness $[I = (R+G+B)/3]$ and colour saturation $[1 - \min(R,G,B)/I]$ of the different elements such as the terrain, water and sky are evaluated for manually segmented

images taken in outdoor environments. It has been evaluated that the average brightness of the sky is two and half times higher than that of the terrain while that of water reflecting the sky is mid-way between the sky and the terrain. Thus, the range information obtained from stereo data could be fused with the terrain type estimated by colour analysis for use in water hazard detection. A colour image classifier based on mixture of Gaussians has been developed under the DARPA Perceptor program and trained on water regions in RGB colour space [21]. The results of testing this classifier on outdoor images reported in [21] suggest that for still water, the classifier accurately labelled the regions of water reflecting the sky, but misinterpreted the pixel reflecting vegetation as vegetation. Some portion of the sky has been mislabelled as water, though this could be avoided with the knowledge of the horizon. The inherent limitation of the classifier includes the need for performing the training at each new site of operation with sufficient number of images containing correctly labelled water bodies. A way of overcoming this limitation by devising a thresholding criteria has been reported in [2].

The main challenges of colour-based classification include

- the inherent ambiguity in the reflectivity spectrum for certain elements such as dry grass and soil
- the colour constancy problem (Colour constancy could be defined as the constancy of the perceived colours of surfaces under changes in the intensity and spectral composition of the illumination [10]) and
- the chromatic shift due to atmospheric effects

2.2.2 Multi-feature based water detection techniques

As colour information is not self-sufficient in labelling water regions, a few works on fusing them with other features such as texture have been reported in the literature [2] [30]. The colour imagery based water cue has already been discussed in section 2.2.1 and hence, the texture and range reflection based cues and their fusing scheme are detailed below.

According to [27], texture quantifies the greyscale intensity variation (contrast) over a region and its directionality. As water regions commonly have a low texture, a 9x9 intensity variance filter is applied over the greyscale intensity image and the resulting image is thresholded in [2] to detect water regions. Texture, like colour is not self-sufficient as it is susceptible to false detections in other cases having low texture such as dirt roads, sky and vegetation.

The range (the distance from the camera to the scene element along the perpendicular to the plane of the image plane) image computed from stereo cameras could be used to detect reflections from water bodies. Reflections of trees and vegetation surrounding a water body could span a portion or all of the water body, depending upon the height of the reflected body

and its distance from the water body. The reflecting water body provides an incorrect range value equal to the range of the actual object being reflected but possesses a value less than the ground elevation on a height image. For example, the pixels corresponding to a nearby puddle reflecting a distant tree would have a large range value equal to that of the tree. Also, their value for elevation (height) with respect to the ground would be below that corresponding to the land along the edges of the water body. Hence, the range reflection could be used as a water cue by scanning along each column in a range image to detect sudden jumps inconsistent with the neighbourhood. However, the water cue from range data is susceptible to false detections on short branches close to the ground surface and in vegetation, where some range data pierces the vegetation.

Assuming the cameras are mounted horizontally, the lower halves of the field of views sense nearby elements while the upper halves sense distant objects. But a nearby water body imaged in the lower half could indicate higher values of depth if it reflects other distant elements such as the sky or a tree. This contradiction in the estimated distance of the water body can also be combined with other features discussed earlier in the multiple cue based approach.

In [2], the water fusion software module merges the water cues from a range-reflection detector, a colour image based sky-reflection detector employing a simple thresholding criteria, a low-texture detector and the zero disparity pixels. Also, any detection above the horizon line or 0.75m above the bottom of the vehicle is discarded to eliminate false matches in the sky and in the tall ground cover.

A multi-feature based water detection approach very similar to the above technique has been reported in [30]. Their technique also employs brightness, texture and range reflection features that are fused to detect water hazards. The brightness and texture cues are first extracted by common image segmentation methods such as region growing and clustering. Then, the pixels exhibiting larger values for range that are inconsistent with those of their neighbourhood and also possessing negative height are detected using the 3D information from stereo. Finally, the features are fused to detect the water regions in the scene. However, it could be inferred that the performance of this technique highly depends on reliable stereo matching which is highly complicated in water regions due to the absence of texture. Moreover, the performance of this approach in labelling distant water bodies is poor as their range values from stereo have larger errors.

Though, a multi-cue based water detection approach offers better results than any technique based on a single feature, the challenging task of formulating a robust fusing scheme capable of accommodating the different factors influencing the appearance of a water body and the increased computational overhead would complicate their use in real time applications.

2.2.3 Short-Wave Infrared (SWIR) imagery

As the absorption coefficient of pure water in the near infrared wavelengths is higher than that in the visible range, water bodies of any appreciable depth appear very dark in the near infrared imagery. This fact coupled with the availability of SWIR cameras with sensitivity from nearly 0.9 to 1.7 μm has motivated the application of passive SWIR imagery in water detection. The research work presented in [21] implies that SWIR is capable of detecting water at moderate angles of incidence and has the potential to discriminate snow and ice from other terrain materials. But the performance of this technique degrades in regions of water strongly reflecting vegetation or the clouds.

2.2.4 Thermal Infrared Imagery

It is obvious that all the above techniques cannot be employed in night operations. It is a well established qualitative observation in the field of remote sensing that water bodies tend to be cooler than their surrounding terrain during the day and warmer at night [21]. The size of water body affects the temperature distribution and smaller bodies equalize temperature quickly while there is significant contrast for larger bodies of water. Moreover, water has a higher emissivity than other terrain materials and hence, improves the contrast during night. The results of the mid-wave infrared imagery (MWIR) based water detection technique employed in [21] show that MWIR certainly offers significant contrast during the period from 12:30 AM to 5:00 AM. However, this technique is limited by the darkening of the water regions near the far shore which is yet to be accounted for.

2.2.5 LASER range finder based approach

The opinion that water bodies do not return signals for robot mounted LADAR ranging systems owing to the specular reflection at the air water interface has been held for several years until [21] was published. It has been suggested that some of the LADAR energy penetrates the interface and could even produce a range measurement of the bottom of the water body depending on the angle of incidence, LADAR wavelength and the attenuation in the water column. Also, the propagation of incident radiation influenced by the above factors has been modelled in [21] enabling us to determine the conditions under which LADAR could be used in detecting water bodies. It has been concluded that within short ranges of shallow water bodies, visible and near infrared LADAR may provide a return value and could be used in detection and depth measurements. Within a certain range (between 6.5 and 11 metres in the simulation of [21]) scene elements other than water provide return values and the absence of return value could be used to characterise water. Beyond this limit, no return signal is obtained from any object and

hence, it is not possible to detect water hazards. The advantage of LADARS is their ability to produce very accurate range data as it helps in discriminating grass of foliage from other smooth surfaces such as rocks or tree trunks based on local range statistics. The fusion of LASER range finder data with colour information has been reported in [29].

2.3 Summary

Starting with a broad overview to the challenging task of outdoor water hazard detection, a detailed insight into the complications associated with this task has been provided. This chapter has then provided a detailed review of the state-of-the-art techniques concerned with outdoor water hazard detection. The following chapter concerns the basic principles behind polarization imaging, the polarization based water detection techniques available in the literature and finally, a detailed description of the proposed system.

Chapter 3

Polarization based vision system for outdoor water hazard detection

Though human vision is incapable of directly visualising the state of polarization of the incoming light, the concepts of polarization have been exploited in many objects used in our day to day life such as polarized sun glasses, digital watches and laptop screens. It is also widely believed that some individuals are sensitive to polarized light, and are able to observe a yellow horizontal line superimposed on the blue sky when staring in a direction perpendicular to the sun's direction (a phenomenon termed Haidinger's brush). Polarization, along with intensity, frequency (or wavelength) and coherence, forms the four fundamental properties of light. As it conveys additional information over intensity and frequency regarding the state of the incoming light, it has the potential to be applied in many computer vision tasks. The interest in applying polarization for water hazard detection is primarily motivated by the fact that the light reflected off dielectric surfaces such as water is partially linearly polarized to a significant degree. Following a detailed discussion of the concepts of polarization and polarization imaging, a review of the state-of-the art water hazard detection techniques based on polarization imaging is provided in this chapter. Finally, the proposed polarization based water detection scheme is discussed.

3.1 Polarization of Light:Background

Transverse waves are characterized by oscillations occurring in a plane perpendicular to the direction of propagation of the wave. Light is a form of electromagnetic radiation with transverse electric and magnetic field components which are oscillating mutually perpendicular to each other. As the magnetic field vector or the electric field vector could be used in characterising the polarization state of the input light, the electric field component alone is discussed in the subsequent sections. Polarization essentially characterises the direction of vibration of this electric field component. If these vibrations are confined to a particular direction or if the vibration along a particular direction is dominant compared to the rest, the light is referred to as plane polarized or partially linearly polarized respectively. On the other hand, if these vibrations are random, the light is declared to be unpolarized.

3.1.1 Types of polarized light

Light propagating along the Z direction has mutually perpendicular time varying electric and magnetic field components confined to the X-Y plane. The resultant of the electric field vector could be split into two components along the X and Y axis as shown below.

$$\begin{aligned}\overline{\mathbf{E}}_x(z, t) &= E_{ox} \cos(kz - wt) \overline{\mathbf{x}} \\ \overline{\mathbf{E}}_y(z, t) &= E_{oy} \cos(kz - wt + \xi) \overline{\mathbf{y}}\end{aligned}\quad (3.1)$$

where E denotes the amplitude of the wave and ξ denotes the phase difference between the two components. Variations in E_{ox} , E_{oy} and ξ lead to different types of polarization, namely, linear, circular and elliptical polarizations as shown in figure 3.1.

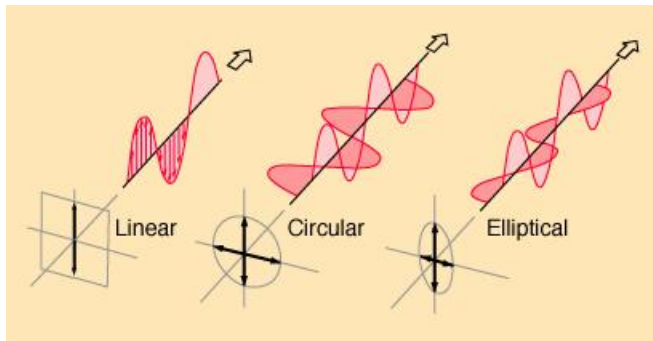


Figure 3.1: Linear, Circular and Elliptical polarization [8]

Case I Unpolarized light When ξ varies in a random manner with time, the light is said to be unpolarized.

Case II Polarized light Simplifying equation 3.1 using trigonometry identities yields the following equation,

$$\left(\frac{E_x}{E_{ox}}\right)^2 + \left(\frac{E_y}{E_{oy}}\right)^2 - 2 * \left(\frac{E_x E_y}{E_{ox} E_{oy}}\right) \cos\xi = \sin^2\xi \quad (3.2)$$

which represents the equation of an ellipse. The linear and circular polarizations are particular cases of the most general elliptical polarization obtained for specific values of ξ .

Linear polarization

In the case of linear polarization, the direction of the electric field remains constant though its amplitude varies with time. The absence of phase difference ($\xi = 0$ or an integral multiple of 180°) between the components E_x and E_y leads to linear polarization. The specific cases of linear polarization include horizontal, vertical and polarization at 45° and are observed when $E_y = 0$, $E_x = 0$ and $E_{ox} = E_{oy}$ respectively [23].

Circular polarization

Circular polarization is observed when the two components of the electric field are of equal amplitude ($E_{ox} = E_{oy}$) but differ in phase by any odd multiple of 90° . Under these conditions, the equation 3.2 of ellipse reduces to

$$\left(\frac{E_x}{E_{ox}}\right)^2 + \left(\frac{E_y}{E_{oy}}\right)^2 = \cos^2\theta + \sin^2\theta = 1 \quad (3.3)$$

which is the equation of a circle. The tip of the resultant electric field vector transcribes a circle as the amplitudes of the field components vary with time. When the source of light is viewed head on and the electric vector rotates in the clockwise or counter clockwise direction, the polarization is labelled to be left or right circular polarization respectively. In either case, the electric field vector completes one revolution per wavelength distance [8].

Elliptical polarization

Unequal amplitudes and the absence of any distinct phase difference between the electric field components result in elliptical polarization. The orientation of the ellipse depends on the ratio E_{ox}/E_{oy} and the eccentricity of the ellipse on ξ .

Case III Partial linear polarization

As the name suggests, this refers to the light which is neither fully polarized nor completely unpolarized. Partially linearly polarized light could be visualized as an unpolarized beam with a certain plane of vibration highlighted in-comparison to the rest. Thus it is essentially the sum of perfectly linearly polarized and completely unpolarized components. This type of polarization serves as the main source of information in the water detection task and hence its

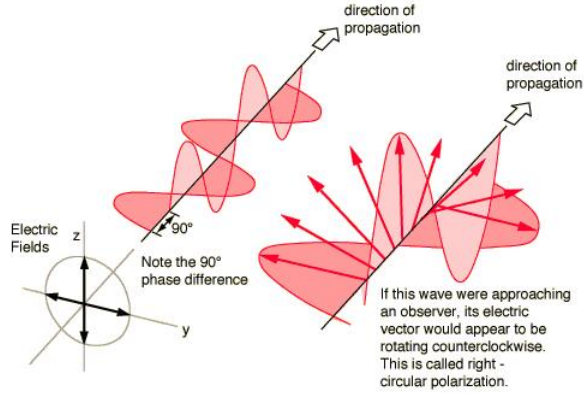


Figure 3.2: Electric field vector distribution in a circularly polarized light [8]

mathematical formulation is discussed in section 3.3. An example for unpolarized and partially linearly polarized lights viewed head on is shown in Figure 3.3.

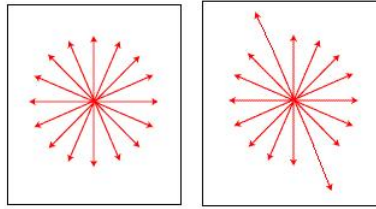


Figure 3.3: Distribution of electric field vectors in an unpolarized and partially linearly polarized light [8]

3.2 Polarization of outdoor light and its analysis

Reflection, scattering, diffraction, absorption, refraction and birefringence (the property of double refraction) are the common physical processes producing polarized light. Of these phenomena, the two principal processes responsible for the abundance of polarized light in natural environments include reflection and scattering [32]. The phenomenon of Rayleigh scattering is responsible for the blue colour of the sky. It is also responsible for the polarization of skylight and the degree of polarization increases with increasing zenith angle from the sun. The consequence of this is that the sky light is significantly polarized when the sun is close to the horizon during sunset and sunrise. As this thesis work concerns water detection in an outdoor environment where the light reflected from the water surfaces is analysed, only the phenomenon

of polarization by reflection is discussed below.

3.2.1 Polarization by reflection

The physical reasoning for the polarization of light upon reflection can be understood by considering the reflection phenomenon as the absorption and re-emission of incident light by oscillating electric dipoles at the interface. As electric dipoles do not emit radiation along the direction of oscillation, only the component of field perpendicular to the direction of oscillation of the dipoles exists in the reflected light. When light gets refracted and specularly reflected at an interface, the dipoles that are produced by the electric field component perpendicular to the interface oscillate along a direction very close to the direction of the reflected beam and hence have a lower value of reflection coefficient. In-particular, when the refracted beam is perpendicular to the reflected beam (which occurs at the Brewster angle), the direction of oscillation of the dipoles induced by the component perpendicular to the interface is along the direction of the reflected beam and hence does not produce any reflected light provided the input light was polarized perpendicular to the plane of incidence. On the contrary, the dipoles induced by the component parallel to the interface will always vibrate along a direction perpendicular to the specular reflection and hence the component parallel to the interface always gets reflected [25] [33].

When electromagnetic radiations encounter an interface between two different dielectrics with different refractive indices (refractive index of a medium is defined as the ratio of the speed of light in vacuum to that in the medium), a portion of it is reflected back into the first medium while the rest is refracted into the other with the sum of their energies equal to that of the incident radiation. In the case of dielectrics (also holds for metals if a complex angle of refraction is considered), the relation between the angle of incidence (equal to the angle of reflection by the law of reflection), angle of refraction and the refractive indices of the two media is given by Snell's law (A.1):

$$n_1 \sin\theta_1 = n_2 \sin\theta_2 \quad (3.4)$$

where n_1 and n_2 denote the refractive indices of the first and second medium while θ_1 and θ_2 denote the angles subtended by the incident and the refracted rays with the surface normal.

The proportions of incident electromagnetic radiation that are reflected and refracted at an interface are quantified by the Fresnel's reflection and transmission coefficients respectively. Following the development of Maxwell's equation for electromagnetic radiation, these coefficients can also be derived from the solutions of Maxwell's equations subject to the boundary conditions at the reflecting interface. The important observation derived from the reflection coefficients is that their values are different for waves parallel and perpendicular to the plane

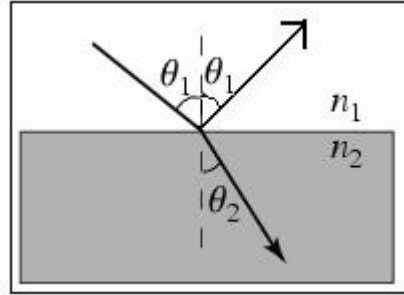


Figure 3.4: Reflection and Refraction at an interface between two media with different refractive indices

of incidence. As seen from figure 3.5, the component perpendicular to the plane of incidence (parallel to the interface between the two media) is reflected to a greater degree in comparison to that parallel to the plane of incidence. Another important observation from the figure 3.5 is that for a particular angle of incidence (labelled as the Brewster angle), the reflection coefficient for the component parallel to the plane of incidence is zero implying the corresponding component of the electric field does not get reflected. When the angle of incidence equals the Brewster angle, the refracted and the reflected rays are at right angles to each other. The Brewster angle of incidence derived from Snell's law in Appendix A is given by

$$\theta_B = \tan^{-1} \left(\frac{n_2}{n_1} \right) \quad (3.5)$$

where n_1 and n_2 denote the refractive indices of the first and second medium shown in figure 3.4.

When an unpolarized light is incident on a flat dielectric surface at the Brewster angle, the component perpendicular to the surface gets suppressed as its reflection coefficient is zero. Thus the reflected light gets completely linearly polarized along the direction parallel to the surface. But for values of incident angles other than the Brewster angle, the reflection coefficient for the component perpendicular to the surface is non-zero though being lower than the corresponding value for the component parallel to the surface. Hence the reflected light gets partially linearly polarized with the degree of polarization varying with the angle of incidence as shown in the Matlab plot for an air-water interface in figure (3.6). As seen from the figure, the degree of polarization is maximum for the Brewster angle (Brewster angle for an air-water interface at $30^\circ C$ is approximately 53°). Common examples of surfaces that reflect polarized light include undisturbed water surface, glass, plastics sheets, and highway roads. This increase in polarization of the reflected light parallel to the reflecting surface is responsible for the annoying glare observed when viewing the distant part of a highway or the surface of a swimming pool on a

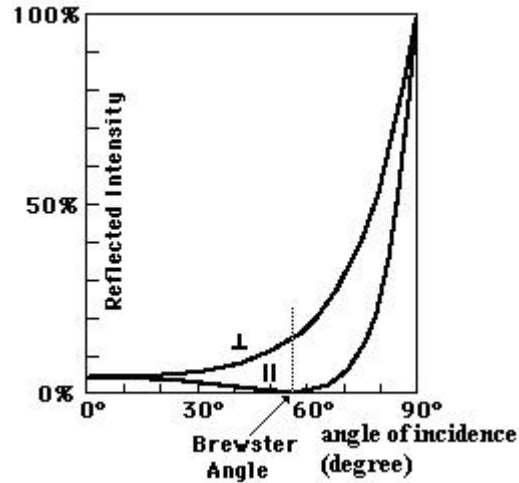


Figure 3.5: Reflected intensity for rays parallel and perpendicular to the plane of incidence.

hot, sunny day.

3.2.2 Analysis of the reflected light using a linear polarizer

A linear polarizer is a device that converts an unpolarized or a mixed polarization beam of light into a linearly polarized beam [24]. Figure 3.7 shows an unpolarized light being linearly polarized by passing through a polarizer as the polarizer does not permit the transmission of components that are not aligned with its transmission axis. The polarizer contains long-chain polymer molecules that are oriented along a particular direction (vertical for the first polarizer and horizontal for the second polarizer) referred to as the transmission axis allowing only the vibrations parallel to their axis to pass through. As a result, an unpolarized light becomes linearly polarized after passing through a polarizer. As seen from figure 3.7, the second polarizer completely blocks the incoming radiation as its axis is oriented perpendicular to the angle of polarization of the incoming light. In case the axis of the polarizer is oriented at an angle with respect to the plane of vibration of the electric field component, it does not completely block the incoming radiation and a portion of the input light reaches the output. This variation in the intensity of the output light with changing orientation of the polarizer is given by the Malus law.

Malus' Law

It states that the intensity of a plane polarized light transmitted through a linear polarizer varies in accordance with the angular separation between the direction of input light polarization and

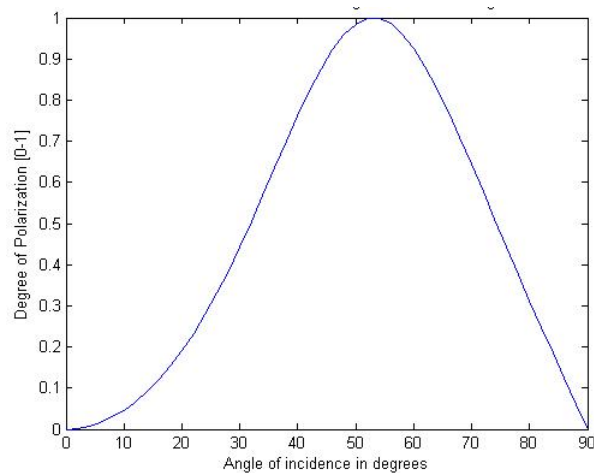


Figure 3.6: Variation of the degree of polarization with angle of incidence of the light reflected at an air-water interface

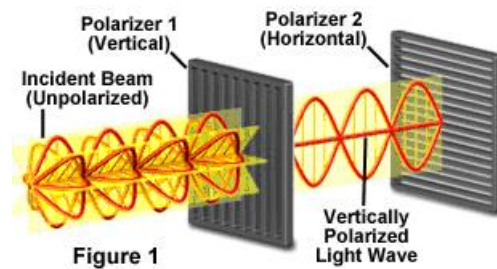


Figure 3.7: Reflected intensity for rays parallel and perpendicular to the plane of incidence.

the transmission axis of the polarizer. The transmitted intensity is quantified by the formula,

$$I = I_0 \cos^2 \alpha \quad (3.6)$$

where I_0 denotes the maximum intensity or irradiance obtained when the transmission axis of the polarizer coincides with the polarization angle of the input light. Thus, rotating the polarizer modulates the intensity of the transmitted light accordingly and in-particular, the transmitted light is completely blanked out when the polarizer is oriented at right angles to the polarization of the input light.

3.3 Mathematical description of partial linear polarization

Stokes vector is a four element column vector capable of representing any type of polarization discussed in section 3.2. Earlier studies reported in [19] indicate that almost all naturally occurring light outdoors and underwater as well as light in indoor environments is partially linearly polarized. Therefore, a simplified scheme capable of completely representing the particular case of partial linear polarization is self sufficient for this thesis work. However, the Stokes vectors and Mueller matrices (used to represent optical elements such as polarizers and retarders) are used to develop a Matlab based graphical user interface in-order to study the state of polarization of the reflected light for different states of polarization of the incident light. It is also worth mentioning that the generalised four element Stokes vector representation capable of describing elliptical polarization offers essential information in other applications such as the determination of surface orientation [17] and discriminating metals from dielectrics [19].

3.4 Simplified polarization imaging

3.4.1 Polarization parameters

In the case of partially linearly polarized light, the three polarization parameters of interest include the light intensity, degree of polarization and the angle of polarization. Light intensity is the quantity perceived by human vision and recorded by imaging sensors as time averaged energy. Hence the other two parameters are essentially a sensory augmentation over human vision. Degree of polarization which is also referred to as partial polarization could be defined as the relative proportion of the linearly polarized component in a partially linearly polarized light. It varies from zero to one corresponding to completely unpolarized and completely linearly polarized light respectively. The orientation of the polarized component in a partially linearly polarized light with respect to a certain reference (say horizontal) is referred to as the angle of polarization. It varies from 0 to a maximum value of 180 degrees.

As discussed under the section 3.2.2, the state of partial linear polarization can be ascertained using a linear polarizer, commonly referred to as the analyzer. Introducing a rotating polarizer in-front of a camera causes the transmitted radiance of the partially linearly polarized light recorded at each pixel of the sensor to vary sinusoidally with a period of 180° in accordance with the polarizer's orientation. In the case of unpolarized light, rotating the polarizer does not cause changes in the intensity of the transmitted light and the sinusoid reduces to a horizontal line with a constant value equal to half of the intensity magnitude of the unpolarized light. On the other hand, partially linearly polarized and linearly polarized incident lights result in

sinusoids having a non-zero and zero values for their minima respectively.

A sinusoid can be uniquely characterised using three points and hence, three different images captured with a polarizer oriented at three different angles between 0 and 180° can be used to completely characterise a linearly polarized light. Following the work of [17] [19] [18], three different intensity measurements (I_0 , I_{90} and I_{45}) were taken at 0°, 45° and 90° and the partial linear polarization parameters are computed as follows:

$$\begin{aligned}
 \text{Phase } \theta &= \left(\frac{1}{2}\right) \tan^{-1}\left[\frac{(I_0 + I_{90} - 2I_{45})}{(I_{90} - I_0)}\right] + 90 \\
 \text{if}(I_{90} < I_0) \text{ (if}(I_{45} < I_0) \theta &= \theta + 90 \text{ ; else } \theta = \theta - 90\text{;)} \\
 & \hspace{15em} (3.7) \\
 \text{Intensity } I &= I_0 + I_{90} \\
 \text{Partial polarization} &= \frac{I_{90} - I_0}{(I_{90} + I_0) \cos 2\theta}
 \end{aligned}$$

The derivations of the formulae in 3.7 are provided in Appendix B. As the angle of polarization is generally defined to be the orientation of the polarizer relative to a reference (horizontal or 0°) at which the minimum intensity is observed, it represents the perpendicular to the actual direction of polarization of the input light. Hence 90° is added to make it parallel to the linearly polarized component.

In many applications, the complete description of the partial linear polarization with all the three parameters discussed above is unwarranted and hence a simplified parameter referred to as the polarization contrast is employed. If O (Orthogonal) and P (Parallel) denote the measurements of the sensor corresponding to two mutually perpendicular orientations of polarizer, then the polarization contrast could be defined as

$$\text{Polarization contrast} = \frac{\|O - P\|}{O + P} \quad (3.8)$$

For example, two measurements (I_{20} and I_{110}) taken with the polarizer oriented at 20° and 110° could be used to compute the polarization contrast shown in 3.8. If the component P aligns with the orientation of the linearly polarized component in the input light, then polarization contrast equals the value of partial polarization computed in 3.7. For all other cases, its values provides a lower bound for the partial polarization.

3.4.2 Polarization imaging cameras

As discussed in section 3.2.2, polarization imaging demands the recording of 2D images corresponding to different orientations of the polarizer (analyser). The choice of the set-up for acquiring polarization images depends on the intended application. The set-ups for acquiring polarization images could be broadly classified into two categories namely, single and multiple

camera set-ups.

Polarization cameras of the early nineties used a monochrome or CCD camera mounted with a mechanically rotating linear polarizer (analyser) which is rotated to three different orientations for complete measurement of partial linear polarization. The advantage of this setup is that the pixels in all the three images are inherently matched and hence enable easier computation of the polarization parameters. However this design is suited only for laboratory studies as it demands mechanical rotation of the polarizer and a static scene. Moreover the mechanical rotation of the polarizer could result in geometric shifting of the projection of the world scene onto the image plane which in turn causes errors in polarization measurement when the scene has significant local intensity variations. To overcome this limitation, Twisted Nematic (TN) liquid crystals which are capable of rotating the polarized component of incident light by a fixed amount could be used along with fixed linear polarizer. In [19], two TN liquid crystals corresponding to 45° and 90° twists are mounted in front of a linear polarizer and their electro-optical switching with an AC signal makes the set-up equivalent to having three different polarizer orientations, namely, 0° , 45° and 90° .

Unlike the single camera set-ups discussed above, multiple camera setups offer the advantage of enabling simultaneous acquisition of the three component images required for polarization imaging. In [17], two cameras mounted with polarizers oriented along mutually perpendicular directions are employed along with a beam splitter and only the polarization contrast parameter 3.8 is computed as three measurements are not available. Though these setups make use of multiple cameras, they do not provide stereo information as all the cameras essentially observe the same scene in the presence of a beam splitter and hence are not suited for use in robot navigation tasks. Using stereo cameras mounted with fixed polarizers oriented along different directions has received increased attention in recent years due to its advantage of enabling stereo vision along with polarization sensing. As the requirement of stereo vision is highly important for robot navigation, the stereo vision based polarization imaging set up is chosen for this thesis work.

3.4.3 Scheme for visualising partial linear polarization

Every pixel in a polarization image is a 3 element vector representing the light intensity, degree of polarization and the angle of polarization. The three components are shown as separate images in figure 3.8 [7]. Hence, a meaningful three dimensional representation scheme is required for visualising the polarization information in the imaged scene.

A hue-saturation-intensity based visualization scheme has been proposed by [20] in which the angle of polarization and partial polarization are mapped into hue and saturation while retaining the intensity as the third component. As the angle of polarization can vary only



Figure 3.8: Images corresponding to intensity, degree and angle of polarization respectively.

between 0° and 180° , it is scaled by two to make it span the entire 360° [3.9]. Coloured pixels in the polarization image imply the presence of linear polarization while colourless pixels indicate unpolarized light. The colour of a pixel determines the angle of polarization (Fig 3.9) and intensity controls the observed brightness of the pixel. The advantage of this representation is that it enables us to visualize the polarization information instead of working with the abstract pixel values for degree and angle of polarization [19].

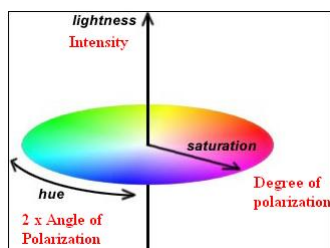


Figure 3.9: HSV colour scale based representation of polarization parameters.

3.5 Suitability of a polarization based water cue for outdoor navigation

Several studies carried out by biologists have confirmed that polarization information is indeed employed by aquatic insects for water detection and in navigation [6]. According to [6], aquatic insects can identify their water habitat by perceiving the partial linear polarization of light reflected from the water surface if the degree of polarization is significant and the direction of polarization approximates horizontal. In spite of these motivations, few works [21] have suggested that applying polarization in robotics will be complicated for cases where the incident light is already partially polarized in context dependent ways. In order to investigate this issue,

an analysis of the state of polarization of the reflected light for different states of the incident light in the context of robot navigation is carried out using the Matlab GUI mentioned earlier in section 3.3.

As discussed under section 3.2.1, an unpolarized incident light upon reflection always becomes partially linearly polarized with the linear component oriented parallel to the reflecting surface (horizontal for a water body). The degree of polarization varies with the angle of incidence as shown in the plot (3.6) reaching its maximum at the Brewster angle. This case applies to water bodies reflecting clouds as the light from the clouds is essentially unpolarized. However if the incident light is partially polarized, then the degree and the angle of polarization of the reflected light is not always parallel to the reflecting surface and they depend on the state of polarization and the angle of incidence of the input light. For example, the light from the blue sky is partially polarized due to Rayleigh scattering with the degree of polarization increasing with increasing zenith angle from the sun and water bodies reflecting the blue sky will not produce horizontally polarized light as those reflecting unpolarized light do.

The following observation conveys that for practical robot applications, it is reasonable to expect the light reflected from water to be partially polarized along the horizontal direction for various possible states of the input light. The plot in figure 3.10 shows that the angle of polarization of the reflected light always lies in the range $\pm 10^\circ$, for the range of incident angles commonly encountered in a robot ($40-70^\circ$ is a reasonable as the cameras in robots are normally mounted with a downward tilt with respect to the horizontal). The value of 0.8 has been used for the value of degree of polarization of the input light in this plot. The other plot in figure 3.11 illustrates that the angle of polarization of the reflected light is further close to the horizontal if the input light is polarized to a lesser extent. In other words, the angle of polarization of the reflected light increases with the degree of polarization of the input light. This analysis could be validated by the work reported in [11] concerning the polarization pattern of the light reflected from freshwater habitats such as ponds reflecting sky and other aspects of the surrounding terrain. It concludes that the polarization of the reflected light is nearly horizontal ($< 10^\circ$) even for portion of the water surface reflecting the partially polarized light from the sky.

However, an exception occurs in the case of a clear shallow water body having shadows as the intensity of the reflected light is very less in this case and the light from the subsurface region dominates. The polarization of light by refraction results in vertically polarized light in contrast to horizontally polarized light with reflection. As the subsurface light gets refracted at the surface before reaching the observer, this component is vertically polarized. Hence, in these cases, the observed light could either be vertically polarized or unpolarized if the vertically polarized refracted light approximately equals the horizontally polarized surface reflected light. Though the angle of polarization is not horizontal, the similarity in its value across a local neighbourhood of the pixels producing partially polarized light could be used to label the water

regions in this case.

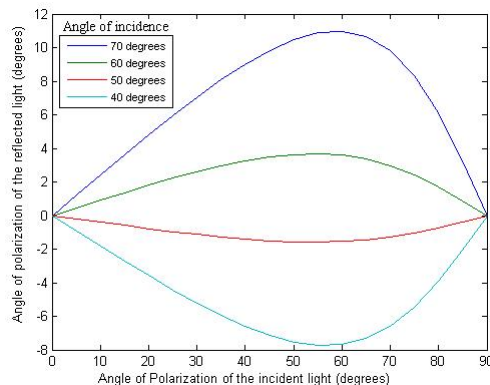


Figure 3.10: Variation of the angle of polarization of the reflected light with that of the incident light having a partial polarization of 0.8 and with angles of incidence equal to 40, 50, 60 and 70 degrees.

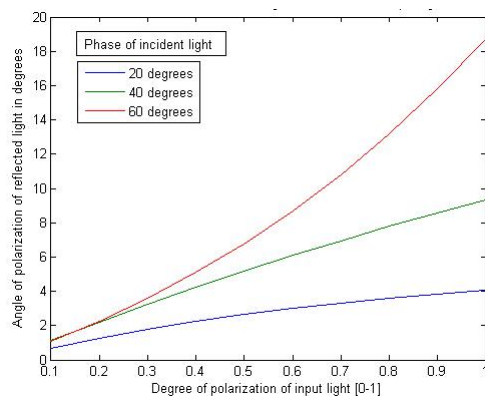


Figure 3.11: Variation of the angle of polarization of the reflected light with the degree of polarization of the incident light having an angle of polarization of 80 degrees and different angles of incidence, namely 20, 40 and 60 degrees.

3.6 Survey of polarization imaging based water detection techniques

Having understood the physics behind polarization imaging, its utility in water detection tasks can now be explored. The idea of applying polarization information in outdoor water detection is the brainchild of the two supervisors of this thesis work specialised in different domains

namely, polarization imaging and robotics, born through a joint discussion. Though the physical principles of polarization are well established as early as the last century, its application in computer vision was explored only in the late eighties [5]. It remained dormant over the next decade mainly due to the fact that commercial video imaging cameras are capable of sensing only intensity and colour. It has gained increased attention only after the development of portable liquid crystal based polarization cameras developed by [18].

An exhaustive literature review reveals that only a few works on polarization based water hazard detection ([22], [3] and [5]) are available till date. The ratio between the intensity images obtained with polarizers oriented along horizontal and vertical directions is computed for every pixel to detect wet roads in [22]. Though this simple approach obtained favourable results when applied to highway environment where most water reflects the sky, it became inaccurate in cases where water reflects other aspects of the terrain such as vegetation [5].

Two different approaches referred to as the single camera system with beam splitting and the three camera method have been attempted in [3]. The former method made use of the Triscene camera set-up from Equinox Corp. that splits the incoming light into three components which are then imaged by three cameras mounted with polarizers oriented along 0, 45 and 90 degrees. The advantage of this approach is that all the three views are registered with sub-pixel accuracy as the cameras essentially view the same scene. As discussed in section 3.4.2, such a set-up cannot be applied in robot navigation as depth information from stereo vision is not possible when all the camera views are record the same 2D image. The latter approach in [3] uses three separate cameras fitted with polarizers oriented at 0, 45 and 90 degrees. This set-up offers the advantage that all the three images can be captured simultaneously. Nevertheless the pixels are not matched and stereo correspondence is required before computing the polarization parameters. This method uses an inherent flat earth assumption and warps two out of the three images to obtain correspondences with the third and hence is not a robust approach suited for practical applications. The other polarization based water hazard detection technique reported in [5] deals mainly with the importance of polarization angle information in water detection and employs a self-adaptive threshold segmentation algorithm and a morphology filtering technique to polarization degree and angle images in order to label the water region. Though the camera arrangement used for image gathering is not explicitly mentioned, it could be inferred from the images that only a single camera based set up has been used.

3.7 Challenges involved in a polarization based stereo system

The inference from the survey discussed in section 3.6 is that a stereo vision based polarization imaging technique for water hazard detection operating without any assumption on the geometry of the outdoor scene elements is yet to be developed. This could be mainly attributed to the increased complexity of computing correspondences between the stereo images obtained with different polarizer orientations. Scene elements reflecting partially polarized light appear with different intensities across the images obtained with different polarizer orientations as seen from figure 3.12 where the reflection from water is completely toned down in the first image due to the polarizer oriented perpendicular to the partially linearly polarized component. Any attempt to process the images to reduce this contrast eliminates the information conveyed by polarization as it is essentially this change in intensity which quantifies the parameters of polarization. Furthermore the reflection of the surrounding scene elements on the surface of water leads to spurious matches between the scene images.



Figure 3.12: Stereo images of an outdoor scene taken from two cameras mounted with polarizers oriented along horizontal and vertical directions highlighting the marked change in intensity of the pixels across the views.

3.8 Functional decomposition of the proposed scheme

The proposed water detection scheme based on stereo vision and polarization imaging essentially includes five stages of processing as seen from the block diagram in figure 3.13. It is intended to investigate two, three and four camera set-ups for analysing the polarization information in the reflected light and finally infer the minimum resource required for optimal performance in outdoor environments. The images recorded by the cameras are then processed using suitable image processing algorithms to improve stereo matching in the following stage. It has been

proposed to try different stereo matching scores and hence choose the score suited for matching across images captured with different polarizer orientations. Once the pixel correspondences across the different views are established, the pixel based polarization parameters are to be computed on a small window around the matched pixel. The computed parameters are displayed using the HSV representation scheme discussed in section 3.4.3 . The level of discrimination between water and other elements of the scene together with the level of similarity among the pixels corresponding to the same water body offered by this approach are to be analysed to determine its suitability in outdoor water hazard detection.

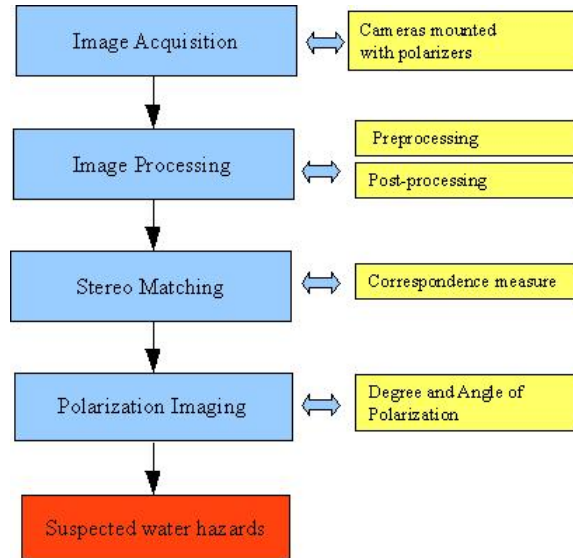


Figure 3.13: Processing blocks of the proposed water hazard detection system.

3.9 Summary

A brief discussion of the essential physics concerning polarization, polarization induced by reflection and the optical component used to analyse partial linear polarization have been provided in sections 3.1 and 3.2. As this thesis work only concerns the analysis of partial linear polarization, the mathematical description of partial linear polarization and ways of visualising it have been discussed in sections 3.3 and 3.4 respectively. Section 3.5 reviews the suitability of applying a polarization based water cue for outdoor navigation. Following a survey of the state-of-the-art polarization based water detection techniques in 3.6, the challenges yet to be overcome in this field are detailed in 3.7. A functional decomposition of the proposed scheme concludes this chapter.

Chapter 4

Implementation and performance evaluation of the proposed schemes

The high level description of the proposed water detection scheme employing principles from stereo vision and polarization imaging was briefed in chapter 3. As the potential for applying polarization information in outdoor navigation is yet to be completely explored, different polarization imaging arrangements starting from a single camera to a four camera setup are to be experimented in this work. It is expected that even if the performance of the proposed system is not robust enough, the results of this investigation would certainly restrict the scope of exploration for future research in this field by directing them to specific problems associated with particular modules discussed in chapter 3.

4.1 Single camera with a rotating polarizer

As discussed under section 3.4.2, a conventional polarization imaging setup involves a single camera mounted with a mechanically rotating polarizer. This set-up is used as a starting point of this thesis work to determine the polarization information conveyed by each pixel of a scene captured with a wide field of view. Care is taken to avoid any mechanical disturbance to the arrangement during the rotation of the polarizer to different orientations. Thus it is reasonable to assume that the pixels across the images with different polarizer orientations are matched and hence the polarization information for various types of static objects such as wet road, vegetation and car windows could be recovered on a pixel basis. Figure 4.1 shows three images

of a scene recorded on a rainy day with polarizers oriented along 0, 45 and 90 degrees with respect to the horizontal respectively. As the images were not acquired simultaneously, the clouds moved by a significant distance between the images and the information from the sky is ignored in the analysis. The objects of interest in this scene include the wet road, the lawn and a few cars seen near the left edge.



Figure 4.1: Images of a scene recorded with polarizers oriented along 0, 45 and 90 degrees with respect to the horizontal respectively.

The three parameters of partial linear polarization namely, the degree of polarization, the phase or the angle of polarization and the intensity are calculated for each pixel from their values in the three component images (Fig. 4.1) using the formulae discussed in section 3.4.1. The three images corresponding to these parameters are shown in figure 4.2. The important inferences that can be derived from these results are as follows:

- The wet road provides higher degree of polarization in-comparison to the rest of the scene elements.
- The bonnet and the windows of the cars also produce high levels of polarized light [the yellowish red spots to the bottom left of the first two images in fig 4.2 correspond to the cars].
- The angle of polarization essentially encodes the surface normal and hence has a uniform value for the wet road as it is horizontal.

The Hue-Saturation-Intensity representation of the polarization image is shown in figure 4.3. The arrow in figure 4.3 points to the cars that are better highlighted after incorporating the polarization information. In-fact they could hardly be distinguished from the other bright objects such as the wet road in the original colour image in figure 4.4 (displayed here to facilitate comparison with the HSV image) and this certainly demonstrates the potential of polarization imaging to characterize a wider range of objects beyond water and hence improve the sensory capabilities of an autonomous vehicle. According to [9], certain aquatic insects often land on

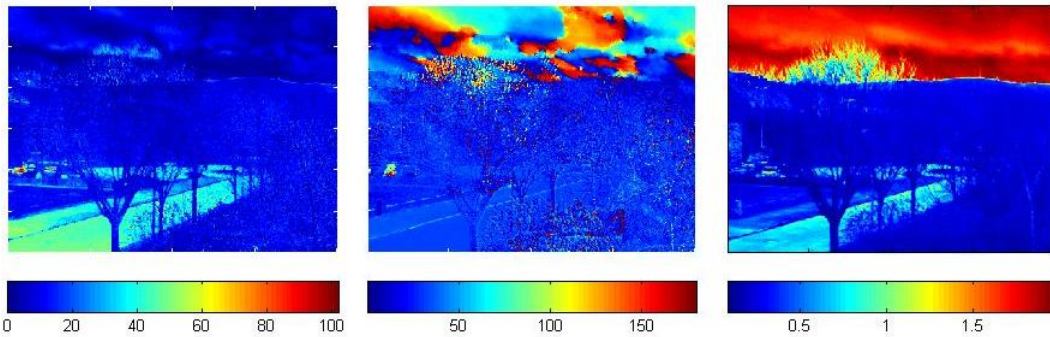


Figure 4.2: Partial polarization, Angle of polarization and Intensity images.

dark coloured cars with shiny surfaces and on shiny horizontal plastic sheets as the light reflected from these surfaces has a high degree of polarization and its angle of polarization is along the horizontal direction. As discussed in section 3.5, certain aquatic insects are polarotactic and are attracted by horizontally polarized light. They [9] measured the polarization state of the light reflected from black, white, red and yellow coloured cars separately in the red, green and blue parts of the spectrum. The results from their study [9] reveal that the degree of polarization of light reflected from red and black cars is high at the blue and green wavelengths and the angle of polarization of light reflected from red and black car roofs, bonnets and boots is nearly horizontal but yellow and white cars provide lower degrees of polarization and their polarization angle is different from horizontal.



Figure 4.3: HSV representation of the polarization image.



Figure 4.4: Original colour image corresponding to a horizontally (0°) oriented polarizer.

The important inference from the single camera set-up is that using a thresholded value of the degree of polarization and the similarity in the angle of polarization across a region in the scene could help in characterising different types of objects which are normally elusive to detection schemes based only on colour information. Though the mechanical rotation of the polarizer can be avoided by using an electrically switched liquid crystal polarizer, the time required for acquiring three images corresponding to different polarizer orientations restrict the applicability of this technique in outdoor navigation. Moreover, 3D information of the scene cannot be recovered using a single camera. So this setup has been used only to establish the ground truth for the polarization information contained in a scene. The images in figure 4.1 have been captured using a AVT Guppy IEEE-1394 / Firewire camera from Edmund Optics Inc and the associated AVT SmartView 1.6.2 software interface. The camera was mounted with a rotating polarizer on a bench and made to look at the scene through the window. The captured images have a Bayer pattern corresponding to CFA (Colour Filter Array Type 2 RGG) and hence have been debayered using the Matlab GUI from [26] by selecting the appropriate pattern.

4.2 Stereo cameras with mutually perpendicular fixed polarizers

In this case, two AVT Guppy Firewire cameras are mounted with mutually orthogonal linear polarizers on a stereo bench and the baseline between them is approximately 4 *cm*. As discussed in section 3.4.1, the parameters of polarization for a partially linearly polarized light cannot be

estimated without a minimum of three intensity measurements taken with different polarizer orientations. As this case involves only two images, the only possible parameter to visualize the polarization information is the polarization contrast discussed in section 3.4.1. According to [14], *sum* and *difference* are the optimum pair (conveying maximum information) of linear combinations of images taken with orthogonally oriented linear polarizers. In other words, the polarization contrast (formula 3.8) parameter representing the ratio of the difference and sum between the two images taken with orthogonal polarizer orientations is the best measure to represent the polarization information in the present case of a two camera setup. But the important design criteria is the choice of the absolute value of orientation for the polarizers.

4.2.1 Choice of orientations for the linear polarizers

As it is known from the principle of operation of the polarizer in 3.2.2 that the polarizer completely blocks the component polarized along the perpendicular to its transmission axis, maximum contrast between the two images can be obtained by orienting one of the two polarizers along a perpendicular to the direction of polarization of the input light. It has been shown in section 3.5 that the light reflected from the water surface is predominantly polarized close to the horizontal direction. Hence, the suitable orientations for the polarizers are along the horizontal and vertical directions. As it is preferred to use a fixed polarizer instead of a rotating polarizer to avoid mechanical disturbance between the acquisitions, two polarizers are fitted with the cameras at fixed orientations. The polarizers are oriented along directions close to horizontal (-15°) and vertical (95°) considering the 0° reference to be the horizon.

It could be noted that a principal component analysis of the polarization statistics of a scene has been performed in [15] to determine the two optimum channels (orientations of the linear polarizing filter) with unequal weighting coefficients instead of using the above mentioned horizontal and vertical directions with equal weighting. This technique referred to as adaptive polarization difference imaging in [15] has been shown to outperform the above measure. This could be attempted in the future to extend the scope of the proposed technique beyond water detection where objects providing light reflected at angles other than horizontal are to be analysed with the requirement of not employing more than two cameras.

4.2.2 Stereo camera calibration

The cameras in the stereo setup are calibrated using the *Matlab camera calibration toolbox* from *J.Y. Bouquet* available at [13]. The main limitation of the stereo setup employed in this work is that the image acquisition from the left and right cameras using the AVT SmartView 1.6.2 software was not simultaneous and moreover, the calibration grid was held in hand. As a result,

the calibration results obtained from the setup had errors. A brief discussion of the essential calibration parameters are provided in Appendix C.

4.2.3 Stereo matching using epipolar geometry

Epipolar geometry eases the problem of searching for correspondences between the stereo images. For any chosen point in one of the two views, it essentially constrains the search space for the corresponding pixel in the other image to a single line referred to as the epipolar line. The matrix which does the transformation between the pixel and an epipolar line is referred to as the Fundamental matrix in an uncalibrated case and as Essential matrix in the calibrated case. The formulation of the fundamental matrix and its relationship with the essential matrix is given in Appendix (C). The task of stereo correspondence can be further simplified by applying a transformation to the stereo images referred to as *image rectification*. Rectification determines a transformation of each image plane such that the pairs of conjugate epipolar lines become collinear and parallel to one of two axes of the 2D images. Thus the task of stereo correspondence is reduced to a 1-D search problem along horizontal lines in rectified images and the corresponding pixels differ only in their column co-ordinate by an amount referred to as the disparity. The value of disparity is inversely proportional to the depth of the 3D point corresponding to the matched pixels. In this thesis work, the stereo images have been rectified using the toolbox from [13]. Optionally, the Epipolar rectification toolkit from [1] could be used to rectify the images by providing the calibration results obtained earlier.

4.2.4 Choice of the matching score

Even in the absence of polarizers which modulate the intensity of light passing through them, locating correspondences in stereo images is complicated due to the fact that the contrast is never identical for a stereo image pair. This could be attributed to the difference in the amount of light entering the cameras due to their different field of views, the differences in the camera settings (aperture, exposure and gain) and the noise in the camera sensors. The addition of a polarizer to the camera further complicates this problem as the scene elements reflecting partially polarized light will certainly appear with different contrast in images captured with mutually orthogonal polarizer orientations.

An exhaustive survey of the state-of-the-art stereo correspondence algorithms is provided in [28]. Two different stereo correspondence scores have been attempted in this thesis work. The other promising candidates for stereo matching across the polarization images that could be attempted in the future works are provided in chapter 5. Due to the interest in extracting as much information as possible from individual pixels, two local window based matching scores have been studied in this work, namely, the Zero mean Normalised Cross Correlation (ZNCC)

and the Census transform. Matlab programs with similar interfaces have been developed for each of these techniques to study their suitability for stereo matching across polarization images.

The Matlab programs on execution display a dialogbox requesting the user for the values of different parameters listed below:

- **Window size for mean filtering:** As the input images are noisy, it is desirable to perform a mean filtering on both of them. As an averaging filter blurs the image, only a 3x3 window is chosen to avoid losing the edges.
- **Window size for computing correspondences:** As the stereo images obtained with polarizing filters have significant variations in the intensity values of the corresponding pixels, it is desirable to choose a window size larger than or equal to 7x7.
- **Starting and final row for locating correspondences:** The calibration errors (section 4.2.2) cause the estimated epipolar lines to differ from the actual ones by one or two rows. Hence, the matching was performed on several rows adjacent to the actual epipolar line to determine the pixel that is best matched to the chosen pixel in the right image.
- **Unicity constraint:** The easiest way to validate the located stereo match in the left image is to compute its correspondence in the right image and check if it corresponds to the pixel selected by the user in the right image. In other words, the stereo correspondences have to be unique and this constraint is referred to as the unicity constraint. In case the unicity constraint fails for the pixel providing the maximum matching score, the pixels which are next to this pixel in terms of the matching score are verified for the unicity constraint. So this parameter request the number of those additional pixels to be examined before deciding that no stereo match is available for the particular pixel.

Following the dialogbox, the programs display the left and right images of the stereo pair and a message box appears asking the user to left click on a pixel in the right image to locate its correspondence in the left image. A mouse pointer is displayed at the current mouse position in the right image and the user can select the pixels using left clicks and once he is finished with pixel selection, he should right click to exit. Whenever a pixel is selected in the right image, it is displayed using a red + sign while its correspondence in the left image is displayed using one of the four possible symbols in figure 4.5 depending on the matching result shown next to the symbols.

The two matching costs that are investigated in this work are detailed below.

Zero mean Normalised Cross Correlation (ZNCC)

If $I_1(u, v)$ and $I_2(u + d, v)$ denote the windows in the stereo rectified images for computing a

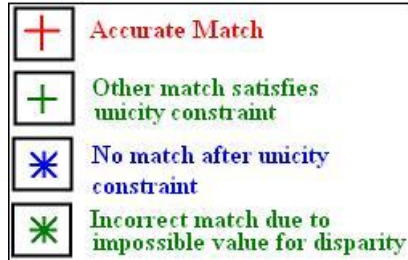


Figure 4.5: Possible results for stereo matching.

matching score corresponding to two candidate pixels with a disparity of d , then the ZNCC score could be computed as follows:

$$\frac{\sum_{u,v} (I_1(u, v) - \bar{I}_1) \cdot (I_2(u + d, v) - \bar{I}_2)}{\sqrt{\sum_{u,v} (I_1(u, v) - \bar{I}_1)^2 (I_2(u + d, v) - \bar{I}_2)^2}} \quad (4.1)$$

Census transform

The census transform belongs to a class of techniques referred to as *non-parametric local transforms* with the other example being rank transform. These techniques were first introduced by R. Zabih [34]. The motivation for using these techniques is derived from the fact that they rely only on the relative ordering of the intensities and not on the intensity values themselves. In other words, these area based approaches provide a dense solution to the correspondence problem through correlation between the statistical information in a neighbourhood. The advantage of this technique over ZNCC is its ability to handle pixels at the boundaries of the objects which involve discontinuities in disparity. The pixels along the boundaries of objects generally exhibit a multi modal statistical distribution as their neighbourhood involves pixels from the object on one side and pixels from the background scene elements on the other and hence are not handled by matching scores based on a uni-modal distribution (ZNCC uses the variance and mean assuming a uni-modal distribution).

The rank transform mentioned above is computed in a windowed region around a pixel as the number of pixels in the neighbourhood whose intensity is less than the intensity of the centre pixel. As census transform offers additional information regarding the spatial distribution of the pixels over rank transform, it has been chosen for this work. The census transform is computed by mapping the local neighbourhood around a pixel to a bit string representing the set of pixels whose intensity is less than that of the centre pixel.

For example, consider the 3x3 local region shown below:

190	200	50
60	110	112
6	10	255

The centre pixel 110 is first compared with 190, and the resulting bit in the bit string is 0 as the pixel has a higher intensity compared to the centre pixel. Following comparisons and concatenation of the resulting bits result the bit string 00110110. As the resulting bitstring is eight bits, it is stored as an eight bit integer. Following the transformation of the stereo images, the matching score in the case of census transform is computed as the “*Hamming distance*” between the windows in the stereo images. The Hamming distance commonly employed in the field of digital communication corresponds to the number of differing pixels between two bit strings. For example, the Hamming distance between 00110101 and 10101111 is 4 as the first, fourth, fifth and the seventh bits differ between the two sequences. As each pixel in a census transformed image corresponds to 8 bit integers, computing the census transform on a 7x7 window can result in hamming distance values from 0 to 384 (calculated as 48x8). The best matching pixel should provide a minimum value for the hamming distance unlike the correlation score where a maximum corresponds to the best match.

4.2.5 Analysis of the stereo matching results

The results of stereo matching with ZNCC and census transform for a window size of 7x7 are shown in figures 4.6 and 4.7. The value of the matching scores for scans along the epipolar lines are displayed in each case. Though both the scores provide equally good matches for pixels on the textured regions of the ground, census transform offers additional matches for pixels on the water surface. Also the degree of confidence in the stereo match is higher with census transform as the peak corresponding to the actual matching pixel is much lower (lower hamming distance corresponds to a better match) than those corresponding to outliers. Hence, census transform is preferred for this work over ZNCC.

4.2.6 Polarization contrast image

As the images have been rectified, it is reasonable to assume that the pixels adjacent to the accurately matched pair of pixels in the two views also correspond to each other. Hence the value of polarization contrast is computed on a 11x11 region around the matched pixel as the ratio of the absolute value of pixelwise difference to that of pixelwise sum between the two views. The resulting polarization contrast information is displayed using hue-saturation-intensity representation in figure 4.8 which is different from the the scheme used for representing the three parameters of polarization in section 3.4.3 as only two values are available for each pixel

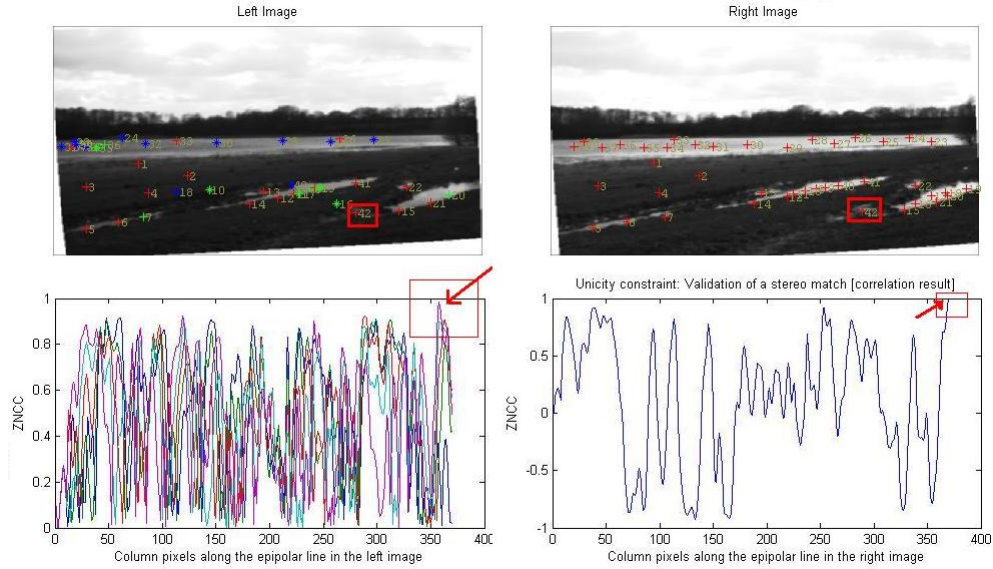


Figure 4.6: The stereo images acquired with approximately perpendicular polarizers, the values of ZNCC along the epipolar line and along the set of rows adjacent to the calculated epipolar line and the unicity constraint validation using the ZNCC scores along the epipolar line of the matched pixel.

in the present case namely, its intensity and the polarization contrast. The intensity component is initialised with the pixel intensities while the hue and saturation components are initialised to be zero matrices. The saturation matrix entries corresponding to the 11x11 region around the matched pixel are alone set to one so that the polarization contrast information appears in colour while the hue matrix is assigned the value of polarization contrast after normalisation by its maximum value. As the values of polarization contrast for pixels on the ground having low values of intensity are not clearly visible, an additional image is displayed where each pixel is computed by adding the normalised value of polarization contrast (normalised by dividing it with its maximum value in the image) to a 5 percent scaled version of the intensity image (so that the scene is visible) and the resulting grey scale 2D image has been displayed using Matlab's *imagesc* function. From the presence of coloured pixels in the first figure, it is evident that polarization contrast provides cues for reflections from water and the inference from the second figure is that the value of polarization contrast is higher for the reflections from water (yellow and cyan) compared to the rest of the ground surface (blue and violet). A non-linear colormap has been chosen for this display as seen from the colorbar in the second image.

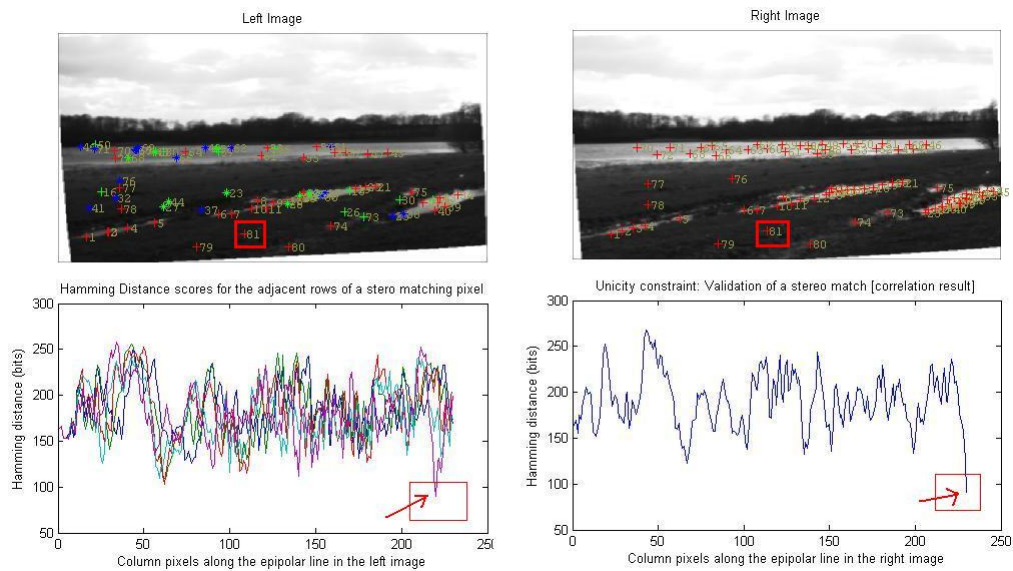


Figure 4.7: The stereo images acquired with approximately perpendicular polarizers, the values of hamming distance along the epipolar line and along the set of rows adjacent to the calculated epipolar line and the unicity constraint validation using the hamming distance scores along the epipolar line of the matched pixel.

4.2.7 Limitations of a stereo polarization imager

The main limitations of a stereo polarization imager discussed above include the following:

- the high level of difficulty in matching pixels obtained from mutually orthogonal polarizer orientations due to the significant differences in their intensities
- the polarization contrast parameter cannot be estimated when the input light is polarized at 45° with respect to the horizontal as the intensities measured with horizontal and vertical polarizers convey the same information resulting in zero contrast
- extending the scope of the proposed work beyond water detection to characterise objects is not feasible without additional information from the polarization parameters such as the degree and the phase of polarization which in turn require a minimum of three cameras with different polarizer orientations

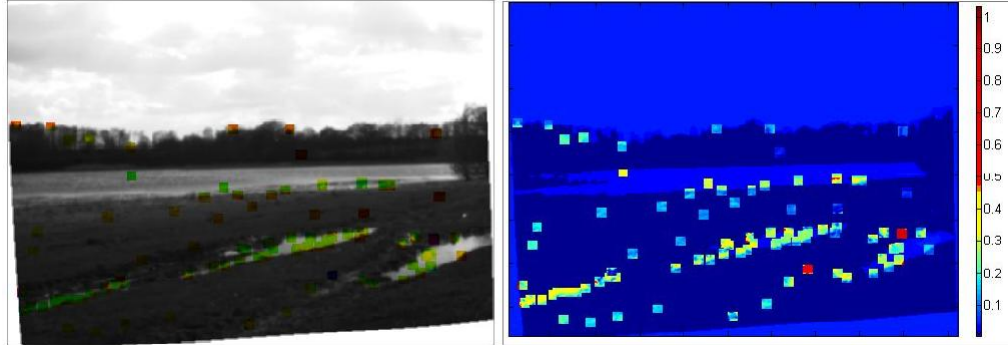


Figure 4.8: Two different schemes for visualizing the polarization contrast computed within a square neighbourhood around the valid stereo matches.

4.3 Water detection using multi-camera polarization imaging

The limitations of the two camera polarization imaging arrangement discussed in section 4.2.7 clearly necessitate a minimum of three cameras for better characterization of the outdoor hazards. But the increased complexity in finding correspondences across the polarization images remains even in the case of a three camera polarization imaging arrangement. Two possibilities to improve the correspondences across the polarization images have been explored and the results of this experimentation are used to propose the minimum number of cameras suited for water detection using polarization imaging.

4.3.1 Four camera polarization imaging arrangement

A likely way to improve the matching across the polarization images is to employ a four camera setup where two cameras are mounted with polarizers oriented along identical directions and hence do not have significant intensity variations while the other two polarizers are oriented along different directions. The proposed approach involves calculating the 3D coordinates of the accurately matched pixels between the views having identical polarizer orientations and hence projecting these points onto the other two views with different polarizer orientations. Four IEEE-1394 cameras from Point Grey Research Inc. [12] mounted with linear polarizers oriented along $0^\circ, 0^\circ, 45^\circ$ and 90° with respect to the horizontal respectively as shown in figure 4.9 are used in the present study. The separation between cameras are 10cm, 20cm and 10cm respectively.

As the rotatable polarizing filters fitted with the cameras were not calibrated, a linear

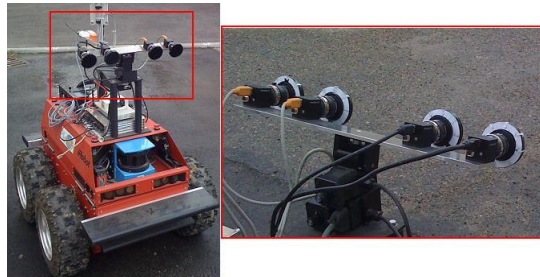


Figure 4.9: The four IEEE 1394 cameras interfaced through the ports in the mobile robot Dala (LAAS, CNRS) and the view of the cameras from behind showing the calibration of the polarizers.

polarizer with a known transmission axis has been used to calibrate them and the rim of the polarizing filter has been labelled with angles relative to its transmission axis as shown by the white labels in figure 4.9. The image acquisition is carried out by interfacing the cameras to the IEEE 1394 ports of the mobile robot Dala from LAAS, CNRS [16] and using the VIAM software module from LAAS which permits simultaneous acquisition of all the four images. The images have then been debayered and finally converted to gray scale for subsequent analysis.

Calibration of the cameras The Matlab calibration toolbox discussed in section 4.2.2 is again used to calibrate the cameras. The sides of the squares measured 81mm for the larger calibration grid used in this case. The steps [1 – 5] listed in Appendix C have to be performed for each camera and the calibration parameters are stored in respective matrices. The distortion in the images is corrected using the calibration parameters. Rectifying the image pairs [1 – 2], [1 – 3] and [1 – 4] results in image 1 being transformed in different ways for the three cases. It is desirable to choose a pixel in the first view and hence search for corresponding pixels in the other three views using epipolar geometry. Therefore it is desirable to work with unrectified images for this four camera set up.

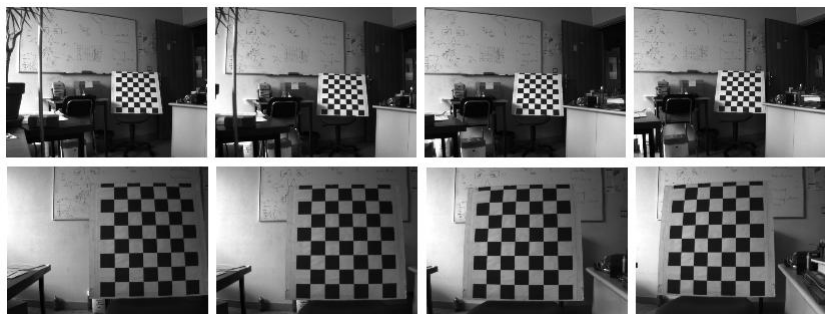


Figure 4.10: Images of the calibration grid corresponding to the four cameras.

4.3.2 The minimum resource required for optimal performance in water detection tasks

The expectation that stereo matching between images having identical polarizer orientations can provide the 3D coordinates of the pixel which could then be reprojected in the other images is found to fail for the case of water reflecting other elements of the surrounding terrain. When water reflects its surrounding scene elements such as vegetation (the mesh structure in figure 4.11), the pixel matches correspond to the reflection of these elements and hence the computed 3D information is incorrect. Moreover, in the case of transparent water bodies, the subsurface structure can get matched resulting in an incorrect value of disparity. Hence adding an additional camera over the conventional three camera polarization imaging arrangement does not ease the challenges associated with the task of stereo matching in these cases. Nevertheless it can ease the problem of stereo matching in other scenarios such as wet roads and water surfaces without reflections from the surrounding scene elements. The performance of the four camera arrangement in these cases will be studied in the future works. It is also required to investigate the four camera setup where the orientations of the two identical polarizers is chosen to be horizontal instead of the vertical direction used in this work.



Figure 4.11: A shallow body of water reflecting the surrounding mesh and other nearby structures.

4.3.3 Water detection using three polarization images

The images which have been captured using the four camera arrangement are used for the analysis in this section and hence all the results display the four images. But only the three images that correspond to different orientations of the polarizers in the four camera arrangement have been used for the computation of the polarization parameters.

The greyscale images captured with different polarizer orientations are displayed in colour using the `imagesc` function in Matlab in figure (4.12). It is evident that the intensities for the water region in the first two images are approximately similar while those in the other two have a significant contrast.

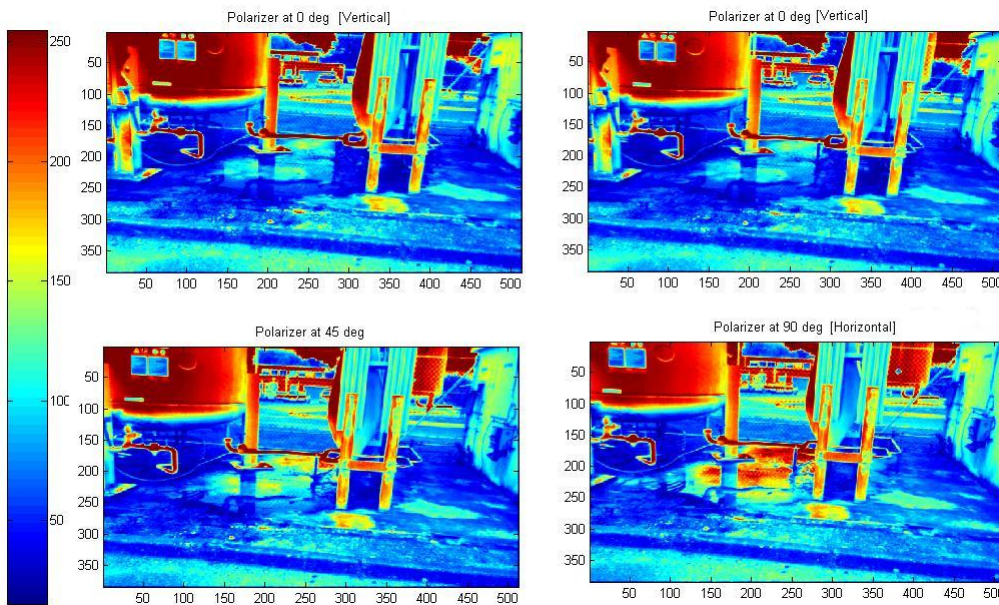


Figure 4.12: Images captured with polarizers oriented along 90° , 90° , 45° and 0° , with respect to the horizontal respectively.

The other alternative proposed to improve the results of stereo matching is the processing of the images corresponding to polarizer orientations other than horizontal as the specular reflection from the water surface are blocked by these polarizers resulting in lower values of intensity for the water regions. The histogram of the pixels corresponding to the water region for the four images are shown in figure 4.13. It could be inferred that stretching the histograms of the first three images would help in matching with the final image. The technique commonly referred to **histogram equalization** in the field of image processing performs this task of spreading out the histogram to improve the local contrast in images. For example, applying the histogram equalization only on these small regions results in the images shown in figure 4.14. Though the level of improvement obtained by applying the histogram equalization to the selected water region cannot be obtained when applying it to the entire image, it certainly offers an improvement in contrast as seen from the results in figure 4.15. In figure 4.15, though the clipped region corresponding to water is displayed for a better visualization of the effect of this technique, the histogram equalization has been applied to the entire images. It is important

to note from the results in figure 4.15 that performing histogram equalization on the final image (the image corresponding to horizontally oriented polarizer) has the detrimental effect of oversaturating the water region. Therefore in this thesis work, the histogram equalization is performed on the images corresponding to the 90° and 45° polarizer images and the processed images are matched with the 0° image.

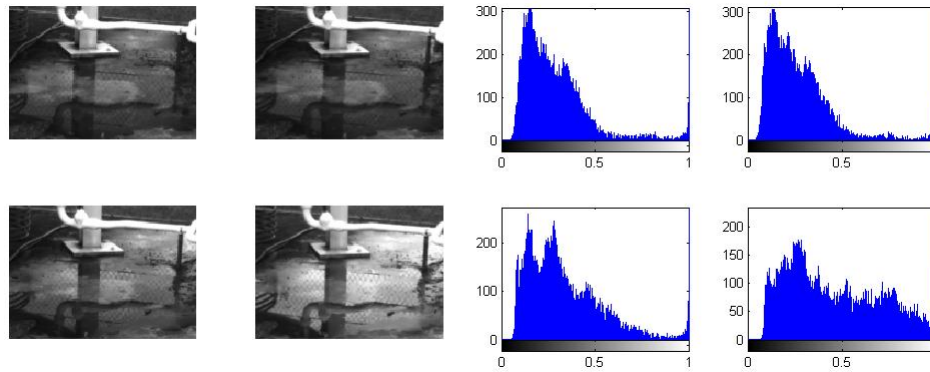


Figure 4.13: Water region clipped from the images obtained with different polarizers oriented at 90° , 45° and 0° with respect to the horizontal and their respective histograms.

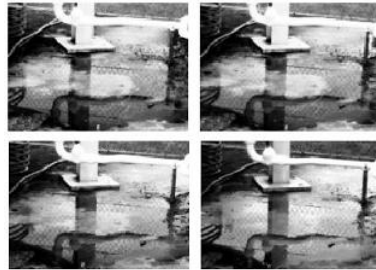


Figure 4.14: The water regions after applying histogram equalization.

A Matlab program has been created to allow the user to select the pixels in the left most image and the corresponding epipolar lines obtained using the fundamental matrices are displayed in all the other images as shown in figure 4.16. After establishing the pixel correspondences which are shown in figure 4.17, the parameters of polarization namely, the degree of polarization and the angle of polarization are computed on windows of size 11×11 around the matched pixels in the three component images and are displayed along with the respective intensities using the HSV representation scheme (figure 4.18) discussed in section 3.4.3.

It could be clearly observed from the HSV image that the light reflected from water is polarized and more importantly, the angle of polarization for all the regions having water is

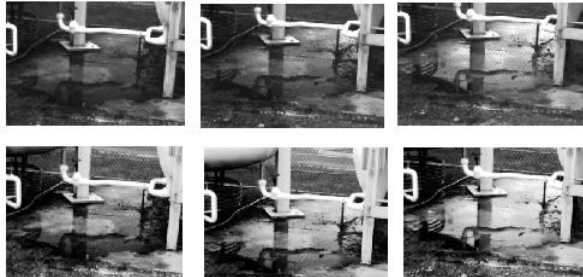


Figure 4.15: Top and bottom rows correspond to the water regions before and after applying histogram equalization to the entire images respectively.

nearly the same as it is observed from the same colour of the squares. This is an important cue that was not available with the polarization contrast parameter calculated from two images. However the angle of polarization for the pixels on the water surface is different from 0° as the cameras were tilted instead of being mounted horizontally to mimic the practical systems. The reason for the presence of a few coloured pixels in regions other than water correspond to incorrect pixel matches. As matching between the pixels obtained from horizontal and vertical polarizer orientations is challenging due to the greater differences in their intensities, it is attempted to first match the pixels in the 90° and 45° image and once a match is established, the window around the matched pixel in the 45° image is then used to search for matches in the 0° image. However, this was not found to provide a phenomenal improvement in the performance.

The inference from these results is that a minimum of three polarization component images are required for obtaining sufficient information required in characterising hazards in outdoor environments. Though census transform provides better matching over ZNCC, the matches in the final image corresponding to the horizontal polarizer still include large number of outliers as seen from figure 4.17. The minimum window size required to obtain at-least a few matches on the surface of the water or along its shore is as large as 11×11 . The development of either a matching score adapted to polarization images or the processing of the input images to enable better matching with conventional matching scores is certainly essential to enable the deployment of the proposed approach in practical systems.

4.4 Summary

This chapter has discussed both the implementation details of different polarization imaging based water detection techniques and the evaluation of their performance. A single camera with rotating polarizer is used to determine the amount of information conveyed by polarization. As



Figure 4.16: The epipolar lines corresponding to the chosen pixels in the top left image are displayed in the other three images.

stereo matching is not required in this case, the polarization parameters can be computed for every pixel from three component images. The results inform that the polarization information has great potential in characterising different objects that cannot be distinguished based on colour information. Following the single camera arrangement, a stereo polarization imaging setup is discussed. The limitations of the two camera setup necessitate the use of at least three cameras in polarization imaging. In order to deal with the challenging task of matching pixels with significant differences in contrast across polarization images, two different proposals have been attempted. The first approach involves the use of an additional camera but it was found to fail for water surfaces reflecting other scene elements. However the performance of the four camera arrangement under other scenarios has to be investigated in the future works. The other technique involving the use of an image processing algorithm, namely, histogram equalization is found to offer certain degree of improvement in stereo matching. The matching scores, namely, ZNCC and census transform have been studied and census transform is found to perform better. Finally, the polarization parameters are computed for windows around the pixels matched using census transform and the potential for a polarization based water cue is demonstrated.

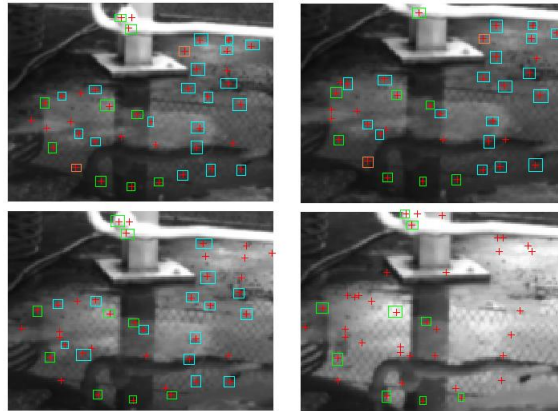


Figure 4.17: The pixels correspondences across the four images with the inliers marked manually using rectangles.



Figure 4.18: HSV representation of the polarization parameters for every pixel within 11x11 square windows around the selected pixels.

Chapter 5

Conclusion and scope for future work

The results of this thesis work convey that polarization imaging has the potential to augment the sensory capabilities of an autonomous vehicle in outdoor environments. In particular, it has the additional capability of discriminating shiny dielectric surfaces from metallic objects as the former provides reflected light with significant degree of partial polarization. In the case of real time applications, a delay caused by the requirement of acquiring several images corresponding to different polarizer orientations is not acceptable and hence, a single camera with a rotating polarizer is not favoured. The two camera polarization imaging arrangement with two mutually perpendicular polarizers contrasts the regions providing either horizontally or vertically polarized light from those reflecting unpolarized light. But the limited information regarding the polarization of the input light provided by this arrangement restricts its usefulness. Therefore, a set of three cameras mounted with polarizers oriented along different directions is recommended for deployment in outdoor navigation tasks. The most challenging aspect of this approach is to establish acceptable number of accurate matches across the different views that contain significant variations in grey scale intensities. A few approaches to improve correspondence across the views such as using an additional camera and the histogram equalization technique are attempted in this work and it is inferred that the latter approach involving post processing of the images is better suited to the particular task of detecting water hazards reflecting the surrounding scene elements. But it is required to investigate the performance of the four camera arrangement under other scenarios and to explore ways of improving the present matching results to obtain optimal performance. The predicted direction for future research in this domain are detailed in the subsequent paragraph.

Firstly, other contrast invariant matching techniques [4] such as those based on multiple frequency channels, phase differences in local regions, mutual information, and graph cuts could be attempted. This thesis work has completely focused on extracting the maximum amount of information at the pixel level and hence higher level processing such as those based on regions have not been carried out. Therefore, the approaches based on matching regions after segmenting the images can be studied. For example, it is known that water surfaces are horizontal and hence it is possible to relate the pixels corresponding to the planar water surface through a homography transformation. This additional constraint can help in improving the correspondence across the views. And finally to generalise the proposed approach to distinguish dielectrics other than water, polarization imaging based on adaptive channels where instead of employing three fixed polarizers, the orientations of the polarizers that provides better contrast between the scene elements can be determined and implemented using a liquid crystal polarizer. It should be noted that this adaptation need not be done for every image acquisition if the field of view of the autonomous vehicle is quite large. Once reliable matching are established between the images, the computed polarization parameters could be fused with other features such as colour and texture to further enhance the sensory capabilities of an autonomous vehicle.

Appendix A

Derivation of the Brewster's angle from Snell's law

Consider a ray of light travelling in a medium of refractive index n_1 and getting partially reflected at the boundary with a medium of refractive index n_2 . If the angle of incidence and refraction are denoted by θ_p and θ_2 respectively, then according to Snell's law

$$n_1 \sin\theta_p = n_2 \sin\theta_2 \quad (\text{A.1})$$

In order to determine the angle of incidence for which the reflected and the refracted rays are perpendicular to each other, set $\theta_p + \theta_2 = 90^\circ$. Substituting the new value of θ_2 as $90 - \theta_p$ in the above equation for Snell's law gives

$$\begin{aligned} n_1 \sin(i_p) &= n_2 \sin(90 - i_p) \\ n_1 \sin(i_p) &= n_2 \cos(i_p) \\ \frac{\sin(i_p)}{\cos(i_p)} &= \frac{n_2}{n_1} \\ \mathbf{i_p} &= \mathbf{\tan^{-1}\left(\frac{n_2}{n_1}\right)} \end{aligned} \quad (\text{A.2})$$

As the light incident at the Brewster angle gets linearly polarized upon reflection, it is also referred to as the polarizing angle [31]. The value of Brewster angle for air-water interface can be calculated by using $n_1 = 1$ and $n_2 = 1.33$, which is approximately 53° .

Appendix B

Derivation of the polarization parameters

Let I_0, I_{45} and I_{90} denote the three polarization component images captured with polarizers along $0^\circ, 45^\circ$ and 90° with respect to the horizontal. The variation in the transmitted radiance sinusoid (with a maximum and minimum values of I_{max} and I_{min} respectively) in accordance with the orientation of the polarizer(ϕ) can be formulated [17] as

$$\frac{I_{max} + I_{min}}{2} - \frac{I_{max} - I_{min}}{2} \cos 2(\phi - \theta) \quad (\text{B.1})$$

The value of the transmitted radiance for the three different polarizer orientations namely $\phi = 0^\circ, 45^\circ$ and 90° can be evaluated by substituting the values of ϕ in the above equation. Upon substituting the values of ϕ and simplification, we get

$$\begin{aligned} I_0 + I_{90} &= I_{max} + I_{min} \\ I_{90} - I_0 &= (I_{max} - I_{min}) \cos(2\theta) \\ I_0 + I_{90} - 2I_{45} &= (I_{max} - I_{min}) \sin(2\theta) \end{aligned} \quad (\text{B.2})$$

Further simplification of the above equation yields the angle of polarization as shown below:

$$\theta = (1/2) \tan^{-1} \left(\frac{I_0 + I_{90} - 2I_{45}}{I_{90} - I_0} \right) \quad (\text{B.3})$$

Also, the degree of polarization can be derived from B.2 as

$$\frac{I_{max} - I_{min}}{I_{max} + I_{min}} = \frac{I_{90} - I_0}{(I_{90} + I_0) \cos 2\theta} \quad (\text{B.4})$$

Appendix C

Description of the camera calibration procedure

The essential camera calibration parameters include the intrinsic and the extrinsic matrices. The intrinsic matrix for each camera is of the form

$$\begin{pmatrix} fc(1) & \alpha_c * fc(1) & cc(1) \\ 0 & fc(2) & cc(2) \\ 0 & 0 & 1 \end{pmatrix} \quad (C.1)$$

$fc(1)$ and $fc(2)$ in the above matrix denote the focal length expressed in units of the horizontal and vertical pixels while α_c encodes the angle between the x and y sensor axes. The two element 2x1 vector cc contains the coordinates of the principle point of the camera.

The extrinsic parameters include the 3x3 rotation matrices and the 1x3 translation vector. In the case of single camera calibration, they refer to the transformation from the reference frame attached to the object (calibration grid) to the camera reference frame. In the case of stereo calibration, they represent the transformation between the cameras.

Information regarding the epipolar geometry is conveyed by fundamental matrix F (in the case of uncalibrated stereo) and the essential matrix E (if the intrinsic matrices are known). The two matrices are related as follows:

$$F = K^{-T} E K'^{-1} \quad (C.2)$$

where T denotes the matrix transpose and K and K' denote the intrinsic matrices of the two cameras.

The main steps involved in calibrating a stereo rig using the toolbox from [13] are summarised as follows:

1. Run the `calib_gui.m` by typing `calib_gui` at the prompt.
2. Load the images of the calibration grid corresponding to the left camera and extract the grid corners. The size of the squares in the grid has to be mentioned for the automatic corner extraction procedure and the one used in this thesis work measured $81mm$.
3. Run the calibration step and analyse the re-projection error for the calibration images.
4. Remove the calibration images causing higher values of re-projection errors and run the calibration again.
5. Save the calibration results and change the default name of the file (`Calib_Results.mat`) to `Calib_Results_Left.mat`.
6. Repeat the above mentioned steps for the right camera and finally, save its calibration results under the name `Calib_Results_Right.mat`.
7. These calibration results contain the intrinsic parameters of the two cameras.
8. Now to compute the stereo calibration parameters, run `stereo_gui.m` by typing `stereo_gui` at the prompt. The stereo calibration results contain the extrinsic parameters, namely, the rotation matrix and the translation vector of the right camera with respect to the left camera.

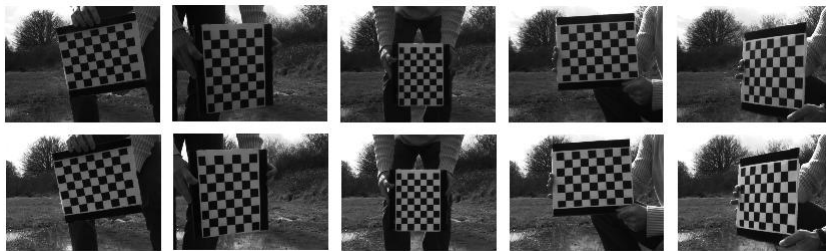


Figure C.1: Image of the calibration grid captured from the left and right cameras of a stereo rig.

Bibliography

- [1] E. Trucco A. Fusiello and A. Verri. Epipolar rectification, 2007. Retrieved from <http://profs.sci.univr.it/~fusiello/demo/rect/>.
- [2] L. Matthies A. Rankin and A. Huertas. Daytime water detection by fusing multiple cues for autonomous off-road navigation. In *Proceedings of the 24th Army Science Conference*, Nov 2004.
- [3] J. Nett A. Sarwal and D. Simon. Detection of small water bodies. Report submitted by PercepTek Robotics 12395 N. Mead Way Littleton, CO 80125, 2004.
- [4] A.S.Ogale and Y.Aloimonos. Robust contrast invariant stereo correspondence. In *Proceedings of the 2005 IEEE International Conference on Robotics and Automation*, 2005.
- [5] H. Pan B. Xie, Z. Xiang and J. Liu. Polarization-based water hazard detection for autonomous off-road navigation. In *Proceedings of the 2007 IEEE/RSJ International Conference on Intelligent Robots and Systems*, San Diego, CA, USA, Nov 2007.
- [6] J. Gál B. Bernáth and G. Horváth. Why is it worth flying at dusk for aquatic insects ? polarotactic water detection is easiest at low solar elevations. *The Journal of Experimental Biology*, 207, 2003.
- [7] Equinox Corp. Three CCD multi-spectral polarimetric camera. Available at http://www.equinoxsensors.com/products/polarization_image.html.
- [8] C.R.Nave. Classification of polarization, 2006. Available at <http://hyperphysics.phy-astr.gsu.edu/hbase/phyopt/polclas.html>.
- [9] P.Boda P.Malik G. Kriskal, Z.Csabai and G.Horváth. Why do red and dark-coloured cars lure aquatic insects? the attraction of water insects to car paintwork explained by reflectionpolarization signals. In *Proceedings of the Royal Society B(2006)*, pages 1667—1671, 2006. Also available from <http://www.ttk.pte.hu>.

-
- [10] D. Hilbert. Color constancy and the complexity of color. Available at www.uic.edu/~hilbert/papers/Colorconstancy.pdf.
- [11] G. Horváth and D. Varjú. Polarization pattern of freshwater habitats recorded by video polarimetry in red, green and blue spectral ranges and its relevance for water detection by aquatic insects. *The Journal of Experimental Biology*, 200, 1997.
- [12] Point Grey Research Inc. Point grey IEEE 1394 cameras. Homepage: <http://www.ptgrey.com>.
- [13] J. Bouguet. Matlab camera calibration toolbox, 2008. Available at http://www.vision.caltech.edu/bouguetj/calib_doc/index.html.
- [14] J.S. Tyo. Optimum linear combination strategy for an n-channel polarization-sensitive imaging or vision system. *Journal of the Optical Society of America A*, 15:359—366, 1998.
- [15] E.N. Pugh Jr. K.M. Yemelyanov, S.S. Lin and N. Engheta. Adaptive algorithms for 2channel polarization sensing under various polarization statistics with non-uniform distributions. Technical report, Department of Electrical and Systems Engineering, University of Pennsylvania Year, 2006.
- [16] LAAS(CNRS). Outdoor robots - DALA. <http://www.laas.fr/~matthieu/robots/dala.shtml>.
- [17] L.B. Wolff. Polarization camera for computer vision with a beam splitter. *Optical Society of America*, 11(11), 1994.
- [18] L.B. Wolff. Applications of polarization camera technology. *IEEE Expert*, 10:30—38, 1995.
- [19] L.B. Wolff. Polarization vision: a new sensory approach to image understanding. *Image and Vision computing*, 15:81—93, 1997.
- [20] L.B. Wolff and T.A. Mancini. Liquid crystal polarization camera. In *Proc. IEEE Workshop on Applications of Computer Vision*, pages 120—127. IEEE Computer society press, 1992.
- [21] P. Bellutta L. Matthies and M. McHenry. Detecting water hazards for autonomous off-road navigation. In *Proceedings of SPIE Conference 5083: Unmanned Ground Vehicle Technology V*, pages 231—242, 2003.
- [22] I. Horiba M. Yamada, K. Ueda and N. Sugie. Discrimination of the road condition toward understanding of vehicle driving environments. *IEEE Transactions on intelligent transportation systems*, 2:610—622, 2001.

-
- [23] N. Manset. Slides on polarization of light: from basics to instruments (in less than 100 slides). Available at <http://www.cfht.hawaii.edu/~manset/PolarisationLightIntro.ppt>.
- [24] O. Morel. Lecture slides on polarization and vision, 2008. Retrieved from <http://www.vibot.org>.
- [25] Spark Notes. Linear polarization and natural light, 2008. Retrieved from <http://www.sparknotes.com/physics/optics/phenom/section3.rhtml>.
- [26] D.Alleysson P.Vandewalle, K.Krichane and S. Süsstrunk. Joint demosaicing and super-resolution imaging from a set of unregistered aliased images, 2000. Available at http://lcavwww.epfl.ch/reproducible_research/VandewalleKAS07/.
- [27] B. Shanmugam R. Haralick and I. Dinstein. Texture features for image classification. *IEEE Transactions on Systems, Man and Cybernetics*, 3:610—622, 1973.
- [28] D. Scharstein and R. Szeliski. A taxonomy and evaluation of dense two-frame stereo correspondence algorithms. *International Journal of Computer Vision*, 47:742, 2002.
- [29] C.Tasmussen T.Hong, T.Chang and M.Shneier. Feature detection and tracking for mobile robots using a combination of ladar and color images. In *IEEE Proc. On Robotics and Automation*, pages 4340—4345, 2002.
- [30] Z.Xiang T.Yao and J.Liu. Multi-feature fusion based outdoor water hazards detection. In *Proceedings of the 2007 IEEE International Conference on Mechatronics and Automation*, Harbin, China, Aug 2007.
- [31] Heriot-Watt University. Brewster’s angle, 2001. Retrieved from <http://scholar.hw.ac.uk>.
- [32] Rüdiger Wehner. Polarization vision - a uniform sensory capacity ? *The Journal of Experimental Biology*, 204, 2001.
- [33] Wikipedia. Brewsters angle, 2008. Available at <http://en.wikipedia.org>.
- [34] R. Zabin and J. Woodfill. Non-parametric local transforms for computing visual correspondence. In *Proceedings of the European Conference on Computer Vision*, pages 151—158, 1994. Revised version available from www.cs.cornell.edu/rdz.